

Review

Photocatalytic Reduction of Carbon Dioxide on TiO₂ Heterojunction Photocatalysts—A Review

Beatriz Trindade Barrocas , Nela Ambrožová and Kamila Kočí *

Institute of Environmental Technology, CEET, VSB-Technical University of Ostrava, 17 listopadu 15/2172, 70800 Ostrava, Czech Republic; beatriz.trindade.martins.vidigal.barrocas1@vsb.cz (B.T.B.); nela.ambrozova@vsb.cz (N.A.)

* Correspondence: kamila.koci@vsb.cz

Abstract: The photocatalytic reduction of carbon dioxide to renewable fuel or other valuable chemicals using solar energy is attracting the interest of researchers because of its great potential to offer a clean fuel alternative and solve global warming problems. Unfortunately, the efficiency of CO₂ photocatalytic reduction remains not very high due to the fast recombination of photogenerated electron–hole and small light utilization. Consequently, tremendous efforts have been made to solve these problems, and one possible solution is the use of heterojunction photocatalysts. This review begins with the fundamental aspects of CO₂ photocatalytic reduction and the fundamental principles of various heterojunction photocatalysts. In the following part, we discuss using TiO₂ heterojunction photocatalysts with other semiconductors, such as C₃N₄, CeO₂, CuO, CdS, MoS₂, GaP, CaTiO₃ and FeTiO₃. Finally, a concise summary and presentation of perspectives in the field of heterojunction photocatalysts are provided. The review covers references in the years 2011–2021.

Keywords: CO₂ reduction; heterojunction nanocomposite; TiO₂; photocatalysis; renewable fuel; valuable chemicals



Citation: Barrocas, B.T.; Ambrožová, N.; Kočí, K. Photocatalytic Reduction of Carbon Dioxide on TiO₂ Heterojunction Photocatalysts—A Review. *Materials* **2022**, *15*, 967. <https://doi.org/10.3390/ma15030967>

Academic Editor: Massimo Calamante

Received: 7 January 2022

Accepted: 25 January 2022

Published: 26 January 2022

Publisher's Note: MDPI stays neutral with regard to jurisdictional claims in published maps and institutional affiliations.



Copyright: © 2022 by the authors. Licensee MDPI, Basel, Switzerland. This article is an open access article distributed under the terms and conditions of the Creative Commons Attribution (CC BY) license (<https://creativecommons.org/licenses/by/4.0/>).

1. Introduction

Since the 18th century, together with the fast development of human society and the extensive use of fossil energy, environmental pollution has become increasingly serious with great environmental, social and economic impacts. Emissions of CO₂ and other greenhouse gases are steadily increasing. The anthropogenic source of greenhouse gas emissions is fossil fuels combustion, mainly coal, natural gas, and oil, along with soil erosion and deforestation. These gases warm the planet by trapping heat in the atmosphere and are the principal factor in global warming. The average increase in temperature since the preindustrial age has already reached almost one degree Celsius, and this rise looks set to continue [1].

The chance of CO₂ transformation into clean fuel could provide a progressive solution for both the future deficiency of fossil fuels and problem with global warming. In recent years, a large number of methods, such as chemical, electrochemical, biochemical, photochemical, and thermochemical techniques, have been developed for converting CO₂ to light hydrocarbons and alcohols [2,3]. Among the varied methods, CO₂ photocatalytic reduction has been receiving great attention and proved to be a promising alternative technology, once it is possible to produce greener gases and/or gases with industrial and fuel applications, using sunlight to activate the semiconductor materials, which result in the photoreduction of gaseous pollutants. This method is one of the promising processes, which not only remove carbon dioxide, but can also transform it into energy valuable products, such as methane, formaldehyde, methanol, CO and other useful compounds [4–7].

Photocatalysis can be defined as a change in the rate of a photochemical reaction by the activation of a photocatalyst (semiconductor) with sunlight or artificial light (ultraviolet or visible radiation). This process is very efficient and attractive from the economical and

eco-friendly point of view. This method is based on the use of a photocatalyst, usually a semiconductor, illuminated with energy equal to or higher than its energy of the bandgap.

It is well known that CO₂ is an extremely stable molecule with high thermodynamic stability, being that its reduction is extremely complicated. The photocatalytic reduction of CO₂ has complex reaction mechanisms and pathways involving a proton-assisted multi-electron reduction process with high energy barriers, complicated activation and CO₂ adsorption, and selectivity of different products as shown in Table 1.

Table 1. Main products of CO₂ reduction and the corresponding potential (pH = 7).

Reaction	E° (V vs. NHE)	Product	Reference
H ₂ O + 2e ⁻ → 2OH ⁻ + H ₂	-0.41	Hydrogen	[8]
CO ₂ + e ⁻ → CO ₂ ^{-•}	-1.90	•CO ₂ ⁻ anion radical	[9]
2CO ₂ + 2H ⁺ + 2e ⁻ → H ₂ C ₂ O ₄	-0.87	Oxalate	[8]
CO ₂ + 2H ⁺ + 2e ⁻ → HCOOH	-0.61	Formic acid	[10]
CO ₂ + 2H ⁺ + 2e ⁻ → CO + H ₂ O	-0.53	Carbon monoxide	[9,10]
CO ₂ + 4H ⁺ + 4e ⁻ → HCHO + H ₂ O	-0.48	Formaldehyde	[8–10]
CO ₂ + 6H ⁺ + 6e ⁻ → CH ₃ OH + H ₂ O	-0.38	Methanol	[9,10]
2CO ₂ + 12H ⁺ + 12e ⁻ → C ₂ H ₅ OH + 3H ₂ O	-0.33	Ethanol	[8]
2CO ₂ + 14H ⁺ + 14e ⁻ → C ₂ H ₆ + 4H ₂ O	-0.27	Ethane	[8]
CO ₂ + 8H ⁺ + 8e ⁻ → CH ₄ + 2H ₂ O	-0.24	Methane	[8–10]

The photocatalytic system for the reduction of CO₂ makes use of a photocatalyst suspension in a solvent with dissolved carbon dioxide, and irradiation with solar energy can drive the photoreduction of CO₂. Hole scavengers, such as H₂O₂, Na₂SO₃/Na₂S, CH₃OH, and triethanolamine, are ordinarily added to the reaction mixture to decrease the electron–hole recombination and avoid reoxidation by generated holes or the oxygen which is produced from water [9].

Inoue et al. reported, in 1979, CO₂ photocatalytic reduction using several semiconductors (dispersed in water) as photocatalysts. They studied TiO₂, WO₃, CdS, ZnO, GaP, and SiC for the photocatalytic reduction of CO₂, and concluded that TiO₂ and SiC materials had higher photocatalytic activity for this reaction [11]. Recently, several photocatalysts, such as TiO₂, g C₃N₄, ZnIn₂S₄, Bi₂WO₆, graphene (GR), CdS, SrNb₂O₆, and ZnO, were investigated for CO₂ photocatalytic reduction. However, the TiO₂ is the most prevalently used due to its chemical stability, resistance toward corrosion, and mainly low cost [12].

TiO₂ has naturally three polymorphic phases: brookite, anatase, and rutile [13]. TiO₂ has a large band gap and, therefore, the solar light utilization rate of TiO₂ is only 4%. Therefore, the photocatalytic performance of TiO₂ using solar energy is limited [14]. TiO₂ has a relatively high recombination rate of photoinduced electron/hole (e⁻/h⁺) pairs [10]; hence, only a fraction of the generated e⁻/h⁺ pairs are available for photoreaction [15–17]. In recent years, there has been an effort to increase the photocatalytic activity of TiO₂. Several strategies have been suggested to efficiently separate pairs of photogenerated electrons and holes in semiconductor photocatalysts, thereby increasing the efficiency of photocatalysis. Some of the most important ones are, for example, doping metals or non-metals, or creating photocatalysts with heterojunction. The formation of heterojunction photocatalysts, where the generated electron–hole pairs are efficiently separated, has emerged as one of the most promising approaches (Figure 1).

A heterojunction is the interface between two diverse materials which has a different band structure, and it can lead to band alignments. Many types of heterojunctions have been studied that are efficient for increasing the photoactivity of materials. These include conventional heterojunctions (type-I, type-II and type-III), surface heterojunctions, p–n heterojunctions, direct Z-scheme heterojunctions, and graphene-semiconductor (graphene-SC) heterojunctions [18]. In the conventional heterojunction photocatalysts, there are three types: the type-I have a straddling gap (Figure 2a), type-II have a staggered gap (Figure 2b), and the type-III a broken gap (Figure 2c).

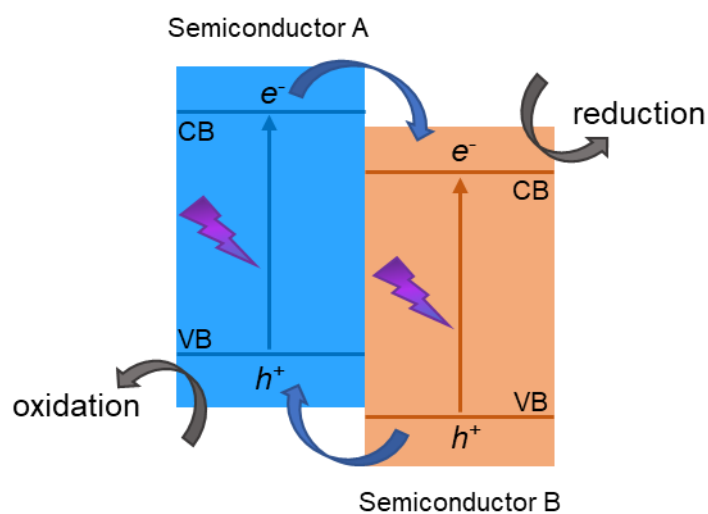


Figure 1. Schematic illustration of the electron–hole separation on an example of heterojunction photocatalyst type-II. Adapted according to refs. [18,19].

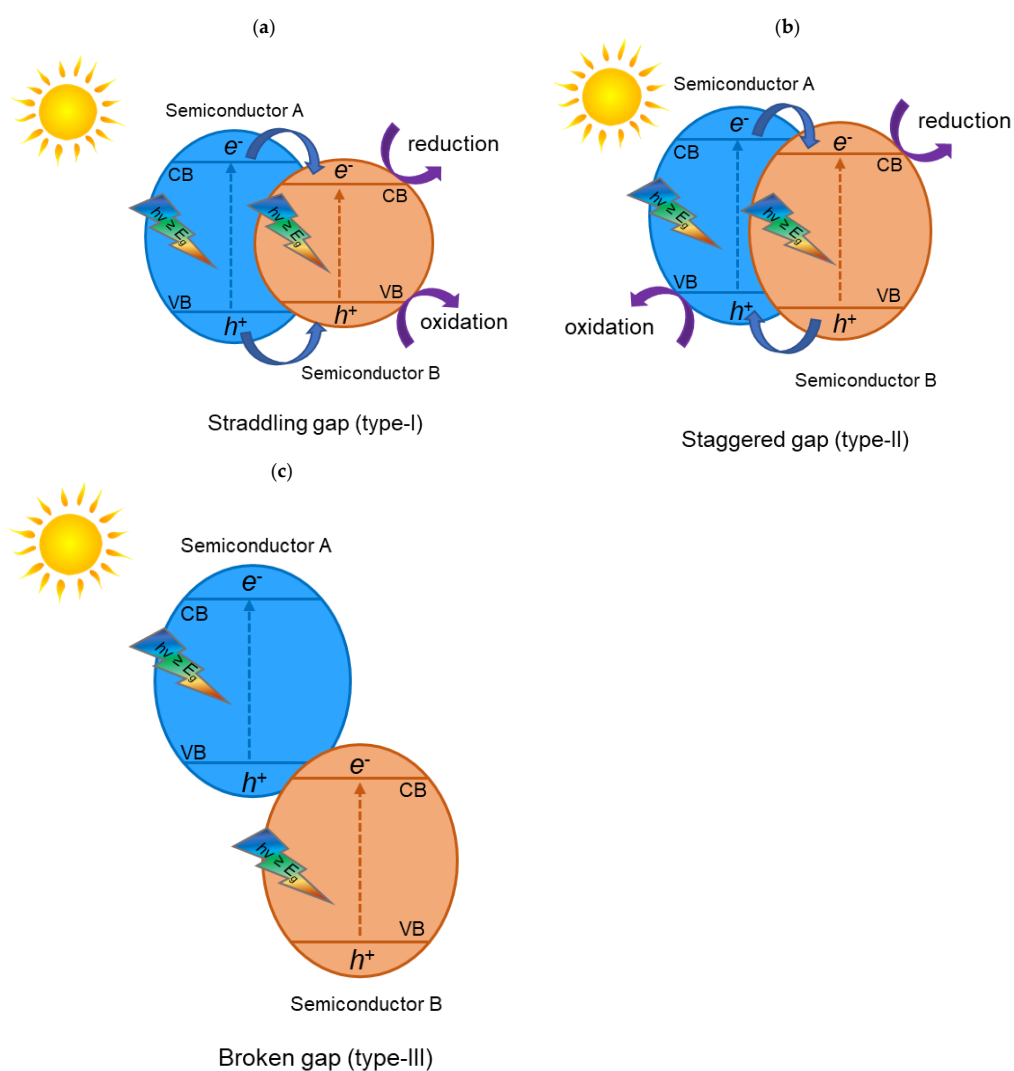


Figure 2. Schematic illustration of the three different types of separation of electron–hole pairs in the case of conventional light-responsive heterojunction photocatalysts: (a) type-I, (b) type-II, and (c) type-III heterojunctions. Adapted according to Refs. [18,19].

Figure 2a shows the type-I heterojunction photocatalyst. The valence band (VB) and the conduction band (CB) of the semiconductor A are, respectively, lower and higher than the matching bands of semiconductor B. For that reason, after irradiation, e^- and h^+ cumulate at the CB and the VB levels of the semiconductor B, which has lower E_g . Since both e^- and h^+ cumulate on one and the same semiconductor, they cannot be effectively separated; therefore, it is not suitable for application in photocatalysis. Figure 2b represents the type-II heterojunction photocatalyst. The VB and the CB levels of semiconductor A are higher than the matching VB and CB levels of semiconductor B. In this case, the migration of photogenerated charges can occur in opposite directions, namely, the e^- are accumulated in one semiconductor, while the h^+ are accumulated in the other semiconductor, resulting in a spatial separation of e^-/h^+ pairs. This separation prevents the rapid recombination of photogenerated charges. A semiconductor with appropriate band positions acts as a scavenger of e^- and h^+ , allowing these charges to react separately. The type-III, as can be seen in Figure 2c, has an architecture similar to the type-II heterojunction photocatalyst; however, there is no overlapping of band gaps, thereby being inadequate for photocatalytic applications [18,19].

The p–n heterojunction (Figure 3) combines the p-type semiconductor and n-type semiconductor. The Fermi level is closer to the valence band in a p-type semiconductor. On the other hand, in the case of an n-type semiconductor, it will shift toward the conduction band [18]. This configuration can increase migration of the electron–hole through the heterojunction for increasing the photocatalytic efficiency by giving an additional electric field. In this type of heterostructure, before light irradiation, the e^- on the n-type semiconductor diffuse across the p–n interface to the p-type semiconductor, abandoning positive holes (h^+). In the meantime, the positive holes of the p-type semiconductor diffuse into the n-type semiconductor, abandoning negative electrons. This diffusion of electrons and holes continues until the Fermi levels of the semiconductors are equal. As a result, an internal electric field is formed on the p–n interface. The electrons and holes, which are photogenerated in p-type and n-type semiconductors, travel due to the impact of the internal electric field from the conduction band of the n-type to the valence band of the p-type, respectively, following the spatial separation of electrons and holes, and prolong their lifetime. Consequently, the efficiency of e^-/h^+ separation in the case of the p–n heterojunction is quicker than that of type-II heterojunction photocatalysts because of the synergic effect of the band alignment and the internal electric field [18]. For instance, it is very often that the combination of TiO_2 (n-type) with a p-type semiconductor for the formation of a p–n heterojunction occurs [10].

However, for these types of heterojunctions mentioned above (conventional type-II and p–n heterojunction types), the redox capability of the photocatalyst is decreased, due to the oxidation and reduction processes take place on the semiconductor with lower oxidation and reduction potentials, respectively [10,18].

Another type of heterojunction is the Z-scheme photocatalytic system. The Z-scheme system for a liquid phase was reported in 1979 by A. J. Bard [20]. Since this discovery, the Z-scheme heterojunctions have become one of the major topics of interest for scientific researchers, to overcome the problems of the abovementioned heterojunction photocatalysts, such as the redox ability of the material [18].

The conventional Z-scheme photocatalytic system is formed with two semiconductors (PS I and PS II), which are not in physical contact, and a dissolved redox mediator consisting of an electron acceptor/donor (A/D) pair (Figure 4a). During the photocatalytic reaction, photogenerated electrons migrate from the CB of the PS II to the VB of the PS I through an A/D pair via following redox reactions.

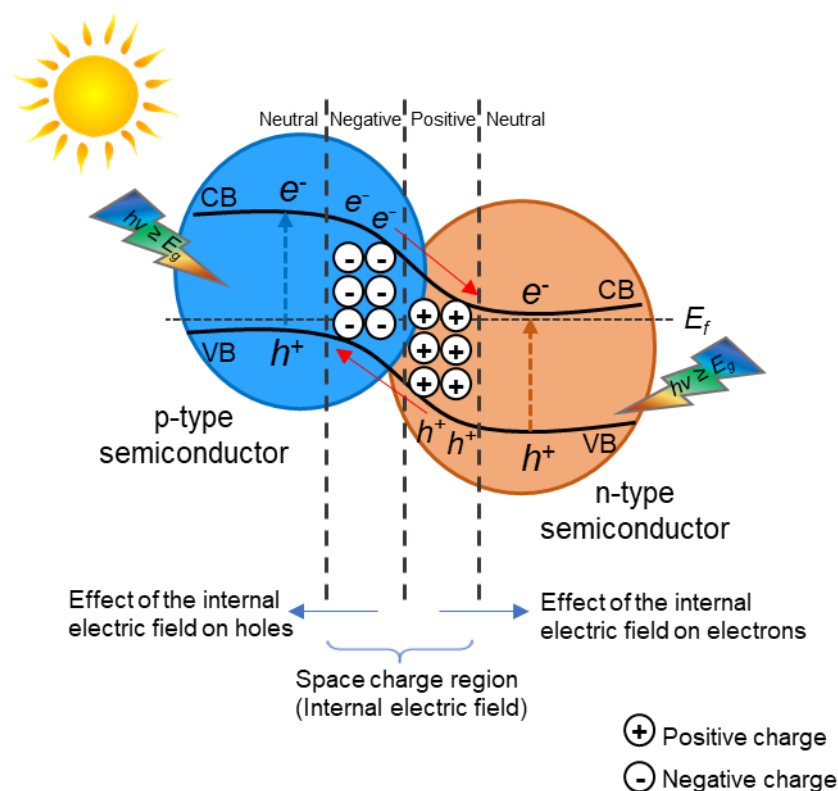


Figure 3. Schematic illustration of the electron–hole separation under the influence of the internal electric field of a p–n heterojunction photocatalyst under light irradiation. Adapted according to Refs. [18,19].

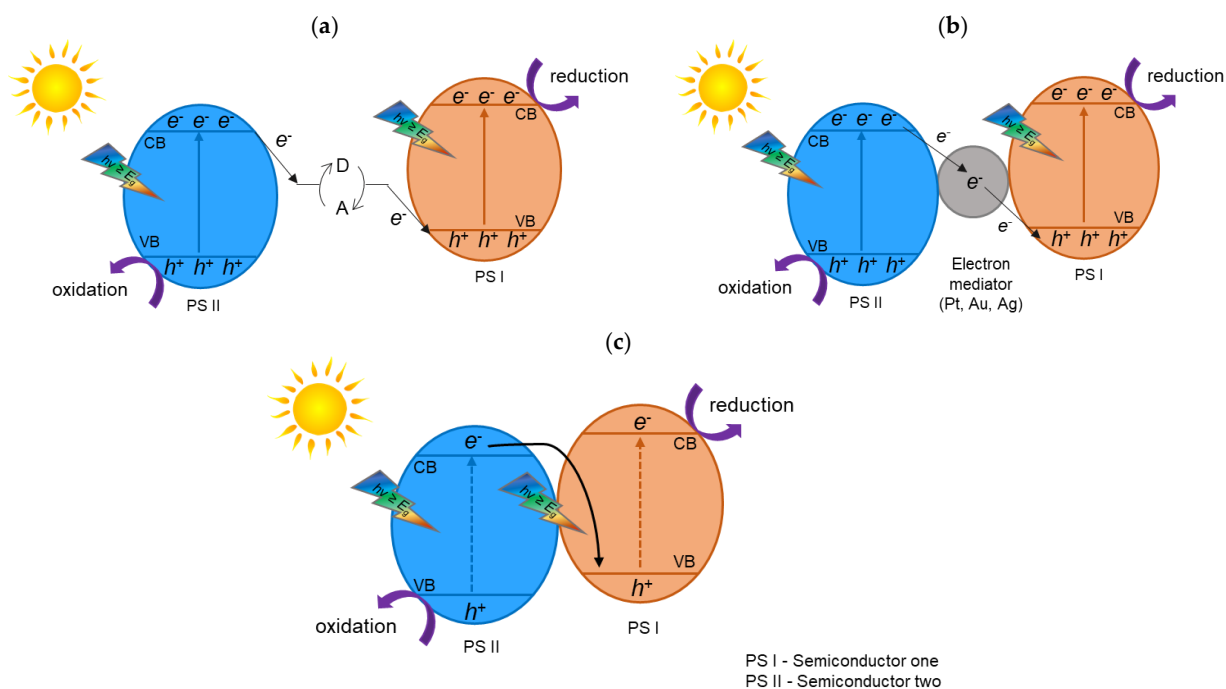


Figure 4. Schematic representation of (a) electron–hole separation on the conventional Z-scheme photocatalytic system; (b) the electron–hole separation on all-solid-state Z-scheme photocatalysts; and (c) electron–hole separation on a direct Z-scheme heterojunction photocatalyst. Adapted according to Refs. [18,19].

The conventional Z-scheme photocatalytic system is formed with two semiconductors (PS I and PS II). Unfortunately, this type of heterojunction photocatalyst has the one limitation; they can solely be used in the liquid phase, in which they are not in physical contact, and an electron acceptor/donor (A/D) pair (Figure 4a), named the redox mediator. In this case, both oxidative and reductive photocatalysts are photoexcited, producing electrons and holes. After that, an e^- photogenerated in the oxidative photocatalyst reacts with the A, forming an electron donor (D) (Equation (1)). Furthermore, a hole in the reductive photocatalyst reacts with the D, producing an electron acceptor (Equation (2)).



Therefore, the acceptor (A) is reduced to a donor (D) when it reacts with the electrons from the conduction band of the photocatalyst I. Then, the donor (D) is oxidized and produces the acceptor (A) due to the reaction with the holes from the valence band.

In this type of heterojunction, electron–hole separation and a redox ability is achieved, due to the fact that electrons are cumulated in photocatalyst I, with higher reduction potential, while holes are cumulated in photocatalyst II, with higher oxidation potential. The conventional Z-scheme photocatalysts can only be constructed in the liquid phase, thereby limiting their wide application in photocatalysis [18,19].

Later, in 2006, Tada et al. [21] suggested a solid-state Z-scheme photocatalytic system consisting of two photocatalysts (PS I and PS II) connected by a solid-phase electron mediator. This mediator can lead the electrons to go from the oxidative photocatalyst to the reductive photocatalyst, eliminating the inactive charge carriers [19]. Furthermore, this system (Figure 4b) can be applied in practically all experimental conditions, markedly extending it using. However, noble metals (such as Pt, Ag, and Au), which are rare and expensive, are used usually as mediators of electrons in this system, being a limitation to their practical application. In addition, this type of mediator can also absorb incident light, decreasing the photocatalyst's light utilization [18,19].

In 2013, Yu et al. [22] suggested a heterojunction photocatalyst with the direct Z-scheme. In this case, there is a combination of two different photocatalysts, without an electron mediator. Figure 4c shows that the construction of this direct Z-scheme is the same as the all-solid-state Z-scheme, except that the rare and expensive electron mediators are not required in this system [18,19]. Similarly, e^- and h^+ are spatially separated on the material with the higher reduction potential and oxidation potential of the direct Z-scheme heterojunction photocatalyst, respectively. The fabrication cost of this direct Z-scheme is low and comparable to that of conventional type-II heterojunction systems. Furthermore, the electron–hole transfer on the direct Z-scheme heterojunction is physically more favorable than that on the type-II heterojunction due to the electrostatic attraction between electrons and holes. In particular, in the case of the direct Z-scheme photocatalysts, the transfer of e^- from the CB of the PS II to the h^+ rich VB of the PS I is easier, due to the electrostatic attraction between the electrons and the holes. Moreover, without the use of liquid-phase or noble metal electron mediators, the direct Z-scheme photocatalysts have greater potential for wide practical applications [18,19].

The structure of a direct Z-scheme catalyst and p–n heterojunction is similar to that of a type-II heterojunction catalyst. For that reason, it is essential to study the charge-carrier migration mechanism for the different types of heterojunction photocatalysts through various characterization methods, so as to differentiate them. Therefore, various characterization methods could be used for this purpose, such as radical scavenging, photocatalytic reduction testing, metal loading, X-ray photoelectron spectroscopy (XPS), effective mass calculation, internal electric-field simulation and effective mass calculation. Using only a single characterization method cannot provide exact information on the charge-carrier migration mechanism for the heterojunction photocatalyst. Therefore, a comprehensive in-

investigation through a combination of different characterization methods is always essential to describe the type of heterojunction photocatalysts [10,18].

In this review, the most promising semiconductors with heterojunction with TiO₂ photocatalysts for CO₂ photoreduction, such as C₃N₄ [23–33], CeO₂ [34–38], CuO [39–43], CdS [44–47], MoS₂ [48–51], and others [52–54], are summarized.

2. TiO₂ Heterojunction Photocatalysts

2.1. g-C₃N₄/TiO₂

Graphitic carbon nitride (g-C₃N₄) is a metal-free organic semiconductor, with special physicochemical properties, such as photocatalytic stability [55], electronic band structure, sufficient negative potential of conduction band, chemical and high thermal stability, and low cost. Due to its optical bandgap size (~2.7 eV), it can be activated by visible light, being an appropriate solar light harvesting photocatalyst [56–58]. However, this has some disadvantages that reduce its photocatalytic activity, such as high recombination of photogenerated charge carriers, low surface area, and low electrical conductivity [59]. These disadvantages can be overcome by combining them with other heterojunction semiconductors. The combination of wide-band TiO₂ and small-band g-C₃N₄ as a visible light sensitizer to create a heterojunction structure can mask the light response of both photocatalysts, due to the special electronic band structure [60,61]. For this reason, we can harvest more light of the sun through a coupling of g-C₃N₄ and TiO₂, forming a g-C₃N₄/TiO₂ heterojunction. In addition to the CO₂ photocatalytic reduction, the resulting heterojunction between TiO₂ and C₃N₄ is used, for example, in the photocatalytic oxidation of NO [62], and for organic pollutants degradation in waste water [63]. CO₂ photocatalytic reduction using g-C₃N₄/TiO₂ heterojunction photocatalysts are tabulated in Table 2.

Shi et al. [25] reported yTiO_{2-x}/g-C₃N₄ heterojunction photocatalysts with efficient solar-driven CO₂ reduction. The 0D/2D heterostructure of oxygen vacancy-abundant TiO₂ quantum dots referred in the g-C₃N₄ (MCN) nanosheets (TiO_{2-x}/g-C₃N₄), were synthesized by in situ pyrolysis of NH₂-MIL-125 (Ti) and melamine with their different mass ratios (g/g) of 5:0.4, 5:0.15, 5:0.1, and 5:0.05. The samples were named yTiO_{2-x}/MCN (y = 8, 3, 2 and 1, which is identical to the % of Ti-MOF out of melamine). All yTiO_{2-x}/MCN photocatalysts showed magnificent photocatalytic reduction performance of CO₂ compared with MCN. The authors concluded that the overall rapid decay of electron–hole pairs was ascribed to the interfacial charge transfer, which was attended by relaxation of recombination mediated by shallow trapped sites. Extremely fast interfacial charge transfers significantly increased charge separation. Thus, e⁻ in shallow trapped sites could be readily trapped by carbon dioxide. Moreover, coupling with the synergetic advantage of powerful visible light absorption, high adsorption of CO₂ and large specific surface area, TiO_{2-x}/g-C₃N₄ demonstrated an excellent CO evolution rate. This research shows detailed insights into optimizing the heterojunction structure for robust solar CO₂ conversion. The 2TiO₂-MCN performed the highest CO formation, roughly five times that of parent g-C₃N₄. These results show that the significant photoreduction performance of CO₂ is also connected with the unique structures, and interface composition of the 0D/2D structure, such as defects in the photocatalyst as well as high specific surface area for enhancing CO₂ adsorption and supporting charge carrier separation. In these experiments, only carbon monoxide and a small amount of hydrogen were detected [25].

Table 2. CO₂ photoreduction using g-C₃N₄/TiO₂ heterojunction photocatalysts.

Photocatalysts	CO ₂ Photoreduction Condition	Yield of Products	Type of Heterojunction	Ref.			
Type	Prepared	Reaction Mixture	Light Source	Conditions	Yield of Products	Type of Heterojunction	Ref.
TiO _{2-x} /g-C ₃ N ₄	Solid state synthesis	CO ₂ (99.999%), 5 mL of solution containing 4 mL of methyl cyanide (MeCN) solvent, 1 mL of triethanolamine (TEOA), bipyridine (bpy) (10 mmol L ⁻¹) and 25 μL of 20 mmol L ⁻¹ CoCl ₂ aqueous solution	300 W xenon lamp	43 mL quartz vessel with a rubber septum; 25 °C; circulation cooling system. Photocatalyst concentration in 1 g L ⁻¹	CO = 77.8 μmol g ⁻¹ h ⁻¹	Type-II NHE pH=7 *	[25]
(0.3/1)TiO ₂ /g-C ₃ N ₄	Simple mechanical mixing of pure g-C ₃ N ₄ and commercial TiO ₂ Evonik P25	CO ₂ with a certified maximum of hydrocarbons less than 1 ppm (SIAD Technical Gases, CZ)	8 W Hg lamp	Cylindrical stirred batch reactor, with internal volume of 355 cm ³ Photocatalyst concentration in 0.28 g L ⁻¹	CH ₄ = 70 μmol g _{cat.} ⁻¹ CO = 23 μmol g _{cat.} ⁻¹ after 8 h	Type-II ‡	[26]
TiO ₂ @g-C ₃ N ₄ -20%	Stirring method	CO ₂ and 50 mL 0.08 mol L ⁻¹ NaHCO ₃ solution	300 W Xe lamp with a 420 nm optical filter	quartz glass tube with a volume of 60 mL Photocatalyst concentration in 1 g L ⁻¹	CH ₃ OH ~50 μmol g _{cat.} ⁻¹ after 4 h	Type-II(see Ref. [27]) -	[27]

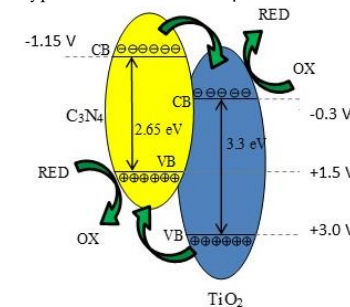
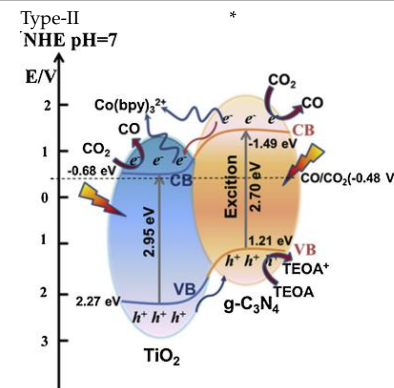


Table 2. Cont.

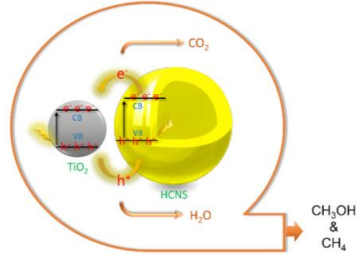
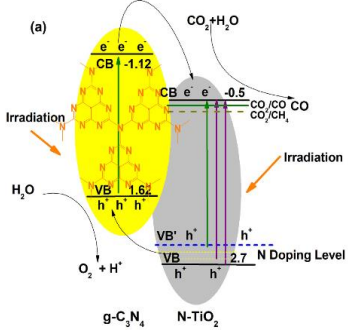
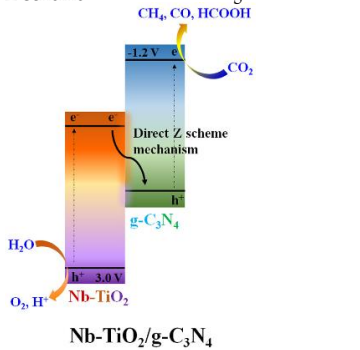
Photocatalysts		CO ₂ Photoreduction Condition			Yield of Products	Type of Heterojunction	Ref.
Type	Prepared	Reaction Mixture	Light Source	Conditions			
HCNS@TiO ₂	Templating method combined with the subsequent kinetically-controlled coating process	CO ₂ (high purity) and H ₂ O (400 mL)	Visible-light (300 W Xenon lamp)	cylindrical Pyrex glass photoreactor with 500 mL of volume Photocatalyst concentration in 1 g L ⁻¹	CH ₃ OH = 52.1 μmol g _{cat} ⁻¹ CH ₄ = 21.3 μmol g _{cat} ⁻¹ after 6 h	Type-II † 	[28]
70:30 g-C ₃ N ₄ -N-TiO ₂	Hydrothermal method and thermal treatment (in situ method)	Deionized H ₂ O + CO ₂ (99.999%)	300 W Xe arc lamp Intensity 100 mW/cm ²	780 mL gas-closed circulation Teflon system Photocatalyst concentration in 0.13 g L ⁻¹	CO = 14.73 μmol after 12 h	Type-II ‡ 	[29]
Nb-TiO ₂ /g-C ₃ N ₄	Solid state synthesis	CO ₂ (99.99%) flow rate 20 mL/min; water vapor was used as hole scavenger	Two 30 W white bulbs	continuous gas system with a reactor (40 mL) located in the center of a dark cover cask using as a reaction chamber (24 L) Photocatalyst concentration in 2.5 g L ⁻¹	CO = 420 μmol g ⁻¹ h ⁻¹ HCOOH = 698 μmol g ⁻¹ h ⁻¹ CH ₄ = 562 μmol g ⁻¹ h ⁻¹	Z-scheme § 	[30]

Table 2. Cont.

Photocatalysts		CO ₂ Photoreduction Condition			Yield of Products	Type of Heterojunction	Ref.
Type	Prepared	Reaction Mixture	Light Source	Conditions			
8 mass % g-C ₃ N ₄ /Ag-TiO ₂	Solvent evaporation followed by calcination	CO ₂ flow rate 3 mL/min; water vapor was used as hole scavenger	300 W xenon lamp	70 mL cylindrical photoreactor Photocatalyst concentration in 0.7 g L ⁻¹	CH ₄ = 28.0 μmol g ⁻¹ CO = 19.0 μmol g ⁻¹ after 3 h		[31]
Phosphate–oxygen (P–O) bridged TiO ₂ /g-C ₃ N ₄	Impregnation-solid state synthesis	CO ₂ + 3 mL H ₂ O; water vapor was used as a hole scavenger	300 W xenon lamp	cylindrical steel reactor (volume of 100 mL and area of 3.5 cm ²) Photocatalyst concentration in 2 g L ⁻¹	CH ₄ = 40 μmol g ⁻¹ h ⁻¹ CO = 15 μmol g ⁻¹ h ⁻¹		[32]
(Au, C ₃ N ₄)/TiO ₂	Immersing (or dipping) method	CO ₂ + 5 mL H ₂ O	300 W Xenon arc lamp	100 mL sealed steel container with cooling water Photocatalyst: Two pieces of samples (0.5 cm ² /sample)	CO = 0.138 μmol cm ⁻² h ⁻¹ CH ₄ = 0.032 μmol cm ⁻² h ⁻¹		[33]

* Reprinted from [25], Copyright (2019), with permission from Elsevier. ‡ Reprinted with permission from [26]. Copyright 2016 American Chemical Society. † Reprinted from [28], Copyright (2020), with permission from Elsevier. ‡ Reprinted from [29], Copyright (2014), with permission from Elsevier. § Reprinted from [30], Copyright (2019), with permission from Elsevier. † Reprinted from [31], Copyright (2017), with permission from Elsevier. ‡ Reprinted from [32], Copyright (2017), with permission from Elsevier. † Reprinted from [33], Copyright (2019), with permission from Elsevier.

Reli et al. [26] studied the $\text{TiO}_2/\text{g-C}_3\text{N}_4$ materials with the ratio of TiO_2 to $\text{g-C}_3\text{N}_4$ ranging from 0.3/1 to 2/1 ($\text{TiO}_2/\text{g-C}_3\text{N}_4$ ratio of 0.3/1, 0.5/1, 1/1, and 2/1) for the photoreduction of CO_2 and photoreduction of N_2O . They reported that the production rate of methane is almost linear during the first 8 h of irradiation; on the other hand, the carbon monoxide yields increased rapidly in the first two hours and then are almost constant. The hydrogen was also detected. The hydrogen is generated from the water splitting. The most photoactive photocatalyst was (0.3/1) $\text{TiO}_2/\text{g-C}_3\text{N}_4$, in the presence of which they observed the highest yields of the products. On the other hand, the lowest product formation was achieved over pristine $\text{g-C}_3\text{N}_4$. The authors concluded that the highest photoactivity of the (0.3/1) $\text{TiO}_2/\text{g-C}_3\text{N}_4$ photocatalyst can be clarified by the combination of several aspects, such as adsorption edge energy, surface area (S_{BET}), crystallite size and efficient charge carrier separation. The key parameter is the efficient charge separation [26].

Zhang et al. [27] described the synthesis of hollow $\text{TiO}_2@\text{g-C}_3\text{N}_4$ nanocomposites for CO_2 photocatalytic reduction under visible irradiation. In this work was reported the utilization of four $\text{TiO}_2@\text{g-C}_3\text{N}_4$ composites with different mass ratios of $\text{g-C}_3\text{N}_4$ with respect to composites of 11.1%, 14.3%, 20% and 33.3%, labeled as $\text{TiO}_2@\text{g-C}_3\text{N}_4$ -11.1%, $\text{TiO}_2@\text{g-C}_3\text{N}_4$ -14.3%, $\text{TiO}_2@\text{g-C}_3\text{N}_4$ -20%, and $\text{TiO}_2@\text{g-C}_3\text{N}_4$ -33.3%, respectively. The results indicated that $\text{TiO}_2@\text{g-C}_3\text{N}_4$ photocatalysts displayed higher photocatalytic activity, compared with pure $\text{g-C}_3\text{N}_4$ and the TiO_2 does not showed photocatalytic activity under visible light irradiation. The increased photocatalytic activity of $\text{TiO}_2@\text{g-C}_3\text{N}_4$ nanocomposites was attributed to the higher photo-induced electron-hole separation efficiency and enhanced photoinduced electron migration. Furthermore, the sample with the best photocatalytic performance for the CO_2 reduction was the $\text{TiO}_2@\text{g-C}_3\text{N}_4$ -20%. They concluded that with the decrease in $\text{g-C}_3\text{N}_4$ content, the yield of methanol decreased, due to the fact that TiO_2 has no catalytic activity in visible light, so the higher amount of TiO_2 weakened the absorbing ability of visible light and reduced the photocatalytic efficiency of the $\text{TiO}_2@\text{g-C}_3\text{N}_4$ -11.1% and $\text{TiO}_2@\text{g-C}_3\text{N}_4$ -14.3% composite materials [27].

Dehkordi et al. [28] reported a hierarchical $\text{g-C}_3\text{N}_4@\text{TiO}_2$ hollow sphere with brilliant activity for CO_2 photocatalytic reduction under visible irradiation. These samples have TiO_2 shell onto the surface of hollow carbon nitride sphere (HCNS) and are named $\text{HCNS}@\text{TiO}_2$. In this work, the photocatalytic efficiency of the $\text{HCNS}@\text{TiO}_2$ photocatalyst was compared with the commercial photocatalyst TiO_2 (P25), $\text{g-C}_3\text{N}_4$ and P25/ $\text{g-C}_3\text{N}_4$. The obtained results showed that the P25/ $\text{g-C}_3\text{N}_4$ and $\text{HCNS}@\text{TiO}_2$ samples had a superior efficiency for the conversion of CO_2 to valuable products under visible light irradiation, once P25 and pristine $\text{g-C}_3\text{N}_4$ showed the small yield of CH_3OH production due to the poor visible light activity and the fast rate of electron-hole recombination, respectively. Furthermore, the heterojunction photocatalyst formed through the combination of TiO_2 and $\text{g-C}_3\text{N}_4$ with a special hierarchical hollow structure ($\text{HCNS}@\text{TiO}_2$) showed to be promising with higher potential than each pristine photocatalysts in the CO_2 . In this reaction, methanol was the primary product in the beginning of irradiation; consequently, the authors concluded that the solar fuel ($\text{CH}_3\text{OH}/\text{CH}_4$) can be obtained by the control of the reaction time of CO_2 photoreduction. The authors concluded that the nanocomposite photocatalytic activity could be ascribed to its special structure, providing properties, such as multiple light reflection, light harvesting, and an improved active site. They also observed that the improvement in the photocatalytic performance of the $\text{HCNS}@\text{TiO}_2$ was obtained due to the increased light absorption. The efficiency of CO_2 photoreduction over the $\text{HCNS}@\text{TiO}_2$ photocatalyst was approximately 5 and 10 times higher than in the presence of pristine $\text{g-C}_3\text{N}_4$ and P25, respectively [28]. The decisive parameter responsible for the increasing the photocatalytic performance of $\text{HCNS}@\text{TiO}_2$ photocatalyst is the synergistic heterojunction creation between the hollow $\text{g-C}_3\text{N}_4$ sphere with TiO_2 , which makes a rapid electron transfer at the interface between HCNS and TiO_2 and increases charge carrier separation [28].

Furthermore, the interest in studying the efficiency of heterojunction materials for CO_2 photoreduction has been increasing, and some studies have also been reported using the combination of $\text{g-C}_3\text{N}_4$ with doped TiO_2 , for instance, TiO_2 doped with amine species (N),

and modified with metals, for example Ag and Au. Therefore, the most relevant reported works are mentioned here in this review.

For instance, Zhou et al. described the selective photoreduction of carbon dioxide to CO, using the graphitic carbon nitride (g-C₃N₄)-N-TiO₂ heterostructure as an effective photocatalyst [29]. In this work, the authors prepared photocatalysts of graphitic carbon nitride and in situ N-modified titanium dioxide (g-C₃N₄-N-TiO₂ composites), using precursors that incorporate urea and Ti(OH)₄ with various mass ratios (80:20, 70:30, 60:40, 50:50, 40:60, 30:70, 20:80, and 10:90). The greater ratios of urea to Ti(OH)₄ (60:40 and more) result in the photocatalysts of g-C₃N₄ and N-doped TiO₂, while smaller ratios (till 50:50) only show in N-doped TiO₂. The selectivity of the photocatalytic reaction is interesting in the presence of these photocatalysts. In the presence of N-doped TiO₂ samples, CH₄ and CO were generated, while in the presence of g-C₃N₄ and N-TiO₂, only CO was performed; the product selectivity may connect with the formed g-C₃N₄. Among the as-prepared samples, 70:30 g-C₃N₄ and N-TiO₂ composites present the highest CO formation, due to the visible light absorption and lowest electrons and holes recombination. As can be seen in the CO₂ photoreduction reactions in Table 1, eight electrons are required for the formation of one CH₄ molecule; however, only two e⁻ are necessary for one CO molecule production. For that reason, the CO₂ photoreduction into CO is a more dynamic, favored process.

Based on this fact and with the obtained results, the authors designed a mechanism for the increase in photocatalytic performance, where charge carriers are created and transmitted between the interface of g-C₃N₄ and N-TiO₂ during irradiation. Therefore, the holes in g-C₃N₄ (h⁺ created in g-C₃N₄ and transmitted from the valence band of TiO₂) might oxidize the H₂O absorbed on the surface of g-C₃N₄, producing O₂ and H⁺. Furthermore, the electrons in N-TiO₂ (created in N-TiO₂ and the e⁻ transmitted from g-C₃N₄) can reduce the CO₂ into C1 intermediates. No methane was produced when a high ratio of urea and Ti(OH)₄ (60:40 or more) was used. This was due to the presence of g-C₃N₄ and N-TiO₂; the H⁺ may not capture the photogenerated e⁻, due to the formation of aromatic heterocycles of g-C₃N₄, which are electron rich, where the protons can be stabilized by the conjugated aromatic heterocycles and, thus, they have difficulty in taking part in the formation of CH₄. Furthermore, the e⁻ in the conduction band of g-C₃N₄ can quickly be transferred to the conduction band of N-TiO₂ for CO₂ photoreduction into CO. For that reason, the g-C₃N₄-N-TiO₂ photocatalyst formed is selective for the production of CO during the CO₂ photoreduction. On the other hand, for low ratios of urea to Ti(OH)₄ (till 50:50), the H[•] radicals or H⁺ ions formatted during CO₂ photocatalytic reduction can be quickly consumed by adsorbed carbon dioxide; thus, CO and CH₄ were simultaneously analyzed, due to the absence of conjugated aromatic system on these samples [29].

Another example of the combination of g-C₃N₄ with doped TiO₂ was reported by Truc et al. [30], using TiO₂ doped with niobium. Truc et al. [30] studied the photoactivity of niobium doped TiO₂/g-C₃N₄ direct Z-scheme photocatalytic system for effective CO₂ conversion into valuable fuels. They prepared three Nb-TiO₂/g-C₃N₄ samples with 25%, 50%, and 75% of the mole percentages of Nb-TiO₂.

The authors observed that g-C₃N₄ did not reduce CO₂ under visible light irradiation, due to the high recombination rates of photoexcited e⁻ and h⁺. However, CO₂ photocatalytic reduction under visible irradiation was possible in the presence of Nb-TiO₂ and Nb-TiO₂/g-C₃N₄ materials, obtaining different products (CH₄, CO, and HCOOH). In the presence of a pure Nb-TiO₂ photocatalyst, the products were CO and CH₄. Nb dopant in TiO₂ lattice led to the creation of the Ti³⁺, which was as an intermediate band between the valence band and the conduction band of the TiO₂, reducing the e⁻ and h⁺ recombination. Furthermore, when the Nb-TiO₂/g-C₃N₄ was used as photocatalyst, not only CO and CH₄ were produced, but also HCOOH was obtained [30].

As expected, the photocatalytic activity for CO₂ reduction was higher for the Nb-TiO₂/g-C₃N₄ samples, when compared to the Nb-TiO₂, g-C₃N₄ and TiO₂ samples. The authors attributed this to the direct Z-scheme mechanism, where photoexcited e⁻ in the Nb-TiO₂ CB combined with the photoexcited h⁺ in the g-C₃N₄ VB avoided the existence of e⁻

in the $g\text{-C}_3\text{N}_4$ CB and h^+ in the Nb-TiO₂ VB. Therefore, this Nb-TiO₂/ $g\text{-C}_3\text{N}_4$ system had more available electron-hole pairs when compared with the pure Nb-TiO₂ photocatalyst. Furthermore, the potential energy of the generated electrons of Nb-TiO₂/ $g\text{-C}_3\text{N}_4$, (~ -1.2 V) was more negative than the generated electron of Nb-TiO₂, (~ -0.2 V), so the generated electron of the Nb-TiO₂/ $g\text{-C}_3\text{N}_4$ required lower energy during the reduction of CO₂ when compared with that of the Nb-TiO₂ [30].

The best photocatalyst for the photoreduction in CO₂ under visible light irradiation was the 50Nb-TiO₂/50 $g\text{-C}_3\text{N}_4$. The higher efficiency of this sample was due to the higher numbers of produced and consumed e^- and h^+ when compared with the Nb-TiO₂ and the other Nb-TiO₂/ $g\text{-C}_3\text{N}_4$ photocatalysts. In the 50Nb-TiO₂/50 $g\text{-C}_3\text{N}_4$ sample, the Nb-TiO₂ mole resembled the mole of $g\text{-C}_3\text{N}_4$; therefore, the photogenerated electrons in the Nb-TiO₂ CB would achieve photogenerated holes in the $g\text{-C}_3\text{N}_4$ VB. Therefore, the amounts of e^- in the $g\text{-C}_3\text{N}_4$ CB and h^+ in the Nb-TiO₂ VB of the 50Nb-TiO₂/50 $g\text{-C}_3\text{N}_4$ sample were considerably higher than in the presence of other photocatalysts. Based on this work, they concluded that the Nb-TiO₂/ $g\text{-C}_3\text{N}_4$ photocatalysts have more charge carriers available for different valuable fuels. Additionally, the produced electrons of the Nb-TiO₂/ $g\text{-C}_3\text{N}_4$ in the conduction band of the $g\text{-C}_3\text{N}_4$, for which the potential energy is around -1.2 V, are enough strong to produce not only CO and CH₄, but also HCOOH during the reduction of CO₂ [30].

Li et al., for example, used the heterostructured $g\text{-C}_3\text{N}_4/\text{Ag-TiO}_2$ photocatalyst for the CO₂ photocatalytic conversion [31]. These authors reported for the first time the preparation of heterostructured $g\text{-C}_3\text{N}_4/\text{Ag-TiO}_2$ materials via a facile solvent evaporation and by a calcination process with $g\text{-C}_3\text{N}_4$ and Ag-TiO₂ as precursors. They prepared four different $g\text{-C}_3\text{N}_4/\text{Ag-TiO}_2$ samples with various masses of $g\text{-C}_3\text{N}_4$ and Ag-TiO₂ and compared them with the commercial TiO₂ photocatalyst (Degussa P25), $g\text{-C}_3\text{N}_4$, and AgTi samples. As expected, the results showed that TiO₂ obtained the lower CO₂ conversion, and no significant amount of CH₄ was formed during the 3 h irradiation. Using $g\text{-C}_3\text{N}_4$, the CO₂ conversion was higher in comparison with TiO₂; however, the CH₄ yields were still very low. The AgTi sample showed higher performance than TiO₂, due to the Ag nanoparticles (NPs) on the AgTi sample not only making the separation of generated charge carriers on TiO₂ by UV irradiation easy, but also increasing the energy of trapped e^- through the Ag surface plasmon resonance effect with the visible light irradiation. Due to this fact, there were more e^- with higher energy for CH₄ formation during CO₂ reduction. Using the CN/AgTi composite samples, both the conversion of CO₂ and solar fuel (CH₄ and CO) yields enhanced with the higher amount of $g\text{-C}_3\text{N}_4$ to AgTi mass ratio from 0 to 8%. They also observed that the rate of electrons consumed was higher when the composite samples were used.

The results showed that the 8CN/AgTi sample (with $g\text{-C}_3\text{N}_4$ to AgTi mass ratio of 8%) obtained the highest photoconversion of CO₂ after 3 h of irradiation. Based on this result, the authors concluded that the coupling of $g\text{-C}_3\text{N}_4$ and AgTi had a synergistic effect in the photocatalytic reduction of CO₂. However, when the $g\text{-C}_3\text{N}_4$ to AgTi mass ratio increased to 12%, this led to an evident decrease in the photocatalytic reduction of CO₂; this decreasing trend is ordinary, and it is possible to attribute it to the fact that an excessive amount of $g\text{-C}_3\text{N}_4$ resulted in shielding of the active site on the TiO₂ surface.

The authors reported that the combination of $g\text{-C}_3\text{N}_4$ and AgTi enhanced the generation of electrons and holes under sunlight. These photogenerated electrons moved through the heterojunction between carbon nitride and titanium dioxide, and further from titanium dioxide to silver nanoparticles with a lower Fermi level, avoiding the electron-hole recombination, and led to electrons cumulating on Ag nanoparticles deposited on the surface of TiO₂ in the $g\text{-C}_3\text{N}_4/\text{Ag-TiO}_2$. After that, the e^- cumulated on the Ag nanoparticles were further energized by the surface plasmon resonance effect. Therefore, the CN/AgTi samples showed higher photocatalytic performance.

The Ag nanoparticles on the TiO₂ surface in the CN/AgTi composite had a significant role once they decelerated the e^-/h^+ pairs recombination due to extracting e^- from conductive band of TiO₂, and also used the surface plasmon resonance effect to increase the energy level of e^- cumulating on the surface. Therefore, the bounteous energetic electrons

on Ag nanoparticles generated from the activation by solar irradiation of the both TiO₂ and g-C₃N₄ parts were answerable for the important synergy of the combination of g-C₃N₄ and AgTi in photoreduction of CO₂ in the presence of water vapor [31].

Liu et al. studied the P–O functional bridges effects on the electron and hole transfer and separation of TiO₂/g-C₃N₄ photocatalysts for the CO₂ reduction [32]. The authors prepared four P–O bridge TiO₂/g-C₃N₄ composite samples with various molar % ratios of phosphate to TiO₂ (1, 5, 10 and 15%) and compared them with the g-C₃N₄ and TiO₂/g-C₃N₄ samples. All photocatalysts exhibited excellent photocatalytic activity for CO₂ reduction, being that CH₄ was the principal product obtained as well as CO in a small amount. The sample TiO₂/g-C₃N₄ with the P–O bridge with 10% molar ratio showed the best performance for this reaction, with photoactivity approximately 2 and 3 times higher than for pure samples. The P–O functional bridges increased the heterojunction coupling between TiO₂ and g-C₃N₄, thereby significantly enhancing the charge transfer and separation, obtaining higher photocatalytic activity.

Based on this study, the authors concluded that the photoactivity of g-C₃N₄ was significantly improved due to the connection with P–O-bridged TiO₂ (in a proper amount). The characterization of the P–O bridge TiO₂/g-C₃N₄ composite samples, using surface photovoltage and photoluminescence spectroscopy, showed that the improvement on the e[−]/h⁺ separation of g-C₃N₄ after coupling with the P–O bridged TiO₂, resulted from the P–O bridge between TiO₂ and g-C₃N₄ that promotes effectively the electrons' transference from g-C₃N₄ to TiO₂ [32].

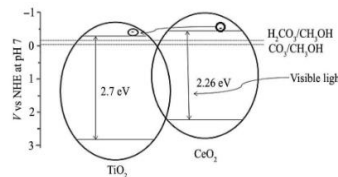
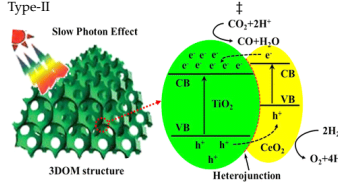
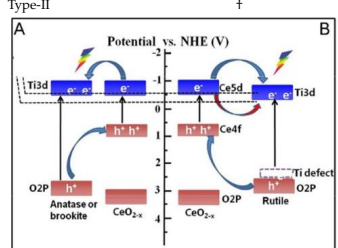
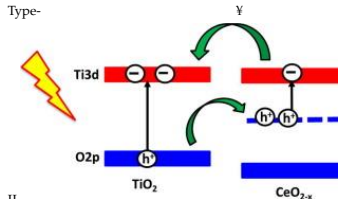
Sun et al. [33] reported the preparation of a Z-scheme heterostructure with r-TiO₂ (rutile) modified with gold and g-C₃N₄ quantum dots to achieve a recyclable and high-efficiency photocatalyst for CO₂ reduction. The photocatalytic activity of (Au, C₃N₄)/TiO₂ composite was compared with the C₃N₄/TiO₂, r-TiO₂, and bulk C₃N₄. The obtained products were CO, CH₄ and O₂; however, using the pristine r-TiO₂ and bulk g-C₃N₄ samples, no significant CH₄ yield was observed. The higher-energy products require a higher reduction potential. Carbon dioxide reduction to methane is an 8-electrons process, which requires the photogenerated charge to have a long lifetime. The CB band of the pure r-TiO₂ is not negative enough to transfer CO₂ to CH₄. However, for the (Au, C₃N₄)/TiO₂ composite, the yield amount of carbon monoxide and methane was markedly enhanced. The authors concluded that a Z-scheme heterostructure was formed at the r-TiO₂ and g-C₃N₄ interface, instead of type-II heterojunction [33].

The results demonstrated that the (Au, C₃N₄)/TiO₂ photocatalyst has four and five times higher photoactivity in comparison with the bulk g-C₃N₄ and pristine r-TiO₂, respectively. This improvement on the photocatalytic performance was attributed to the excellent Z-scheme heterojunction formed in the interface of r-TiO₂ and g-C₃N₄ [33].

2.2. CeO₂/TiO₂

Ceria or cerium oxide (CeO₂) is a rare earth metal oxide that has attracted the interest of researchers due to the fact that the valences of ceria, such as Ce⁴⁺ and Ce³⁺, enhance light absorption ability and increase electron transfer. This material is an n-type semiconductor with a large bandgap energy (2.7–3.2 eV), non-toxic, readily available, and chemically stable [64]. CeO₂ present two oxidation states, Ce (IV) and Ce (III), which give it unique chemical, mechanical, and magnetic properties. Furthermore, the Ce (III) and Ce (IV) oxidation states can be easily converted from one to another [64,65]. The surface oxygen vacancies of CeO₂ from the reversible characteristics of Ce³⁺ and Ce⁴⁺ can promote its photocatalytic performance. During the reduction of Ce⁴⁺ ions into Ce³⁺, there occurs a formation of oxygen vacancies on the photocatalyst surface, which consequently act as electron trap centers that can inhibit the recombination [64]. Recently, the utilization of CeO₂ as a coupling was reported since the Ce⁴⁺/Ce³⁺ displacement can accelerate the charge separation and impurity levels caused by CeO₂ coupled TiO₂ to be excited in the visible region [66]. CO₂ photocatalytic reduction using CeO₂/TiO₂ heterojunction photocatalysts are tabulated in Table 3.

Table 3. CO₂ photoreduction using CeO₂/TiO₂ heterojunction photocatalysts.

Photocatalysts		CO ₂ Photoreduction Condition			Yield of Products	Type of Heterojunction	Ref.
Type	Prepared	Reaction Mixture	Light Source	Conditions			
Mes-CeTi-1.0	Template method using a nanocasting route	CO ₂ + H ₂ O	Xe arc lamp 300 W	stainless steel reactor (volume of 1500 mL) Photocatalyst concentration in 0.07 g L ⁻¹	CH ₄ = 11.5 mmol g _{cat} ⁻¹ CO = ~70 mmol g _{cat} ⁻¹ after 325 min	-	[34]
CeO ₂ -TiO ₂	Stirring method and calcination method	CO ₂ and 300 mL of 0.1 mol L ⁻¹ NaOH solution (for 30 min before irradiation) During irradiation CO ₂ was continuously bubbled	Visible light—500 W Xenon lamp, and 2 mol L ⁻¹ sodium nitrite solution (to remove UV light)	Pyrex glass reactor (500 mL) Photocatalyst concentration in 1 g L ⁻¹	CH ₃ OH = 18.6 μmol g _{cat} ⁻¹ after 6 h	Type-II 	[35]
CeO ₂ /TiO ₂ -4	Gas bubbling-assisted membrane precipitation (GBMP) method	CO ₂ and H ₂ O	300 W Xe lamp and an optical filter with the absorbed light wavelength of <420 nm	Glass reactor (basal diameter of 4 cm) Photocatalyst amount 0.1 g	CO = 2.06 μmol after 6 h	Type-II 	[36]
CeO ₂ /TiO ₂ (R-TiCe _{0.1})	Hydrothermal method	CO ₂ and H ₂ O (Gaseous CO ₂ of 8 kPa was in situ produced by the reaction of NaHCO ₃ with a H ₂ SO ₄ solution (0.5 M).)	500 W Xenon lamp	reactor connected with mechanical vacuum pump Photocatalyst amount 10 mg	CO = 61.9 μmol g ⁻¹ CH ₄ = 23.5 μmol g ⁻¹ after 6 h	Type-II 	[37]
0.2CeO ₂ /TiO ₂	One-pot hydrothermal method	CO ₂ and H ₂ O (Gaseous CO ₂ of 8 kPa was produced in situ by the reaction of NaHCO ₃ with a H ₂ SO ₄ solution (0.5 M).)	300 W Xenon lamp	reactor connected with mechanical vacuum pump Photocatalyst amount 10 mg	CO = 46.6 μmol g ⁻¹ CH ₄ = 30.2 μmol g ⁻¹ after 6 h	Type- 	[38]

* Reprinted from [35], Copyright (2015), with permission from Elsevier. ‡ Reprinted with permission from [36]. Copyright 2014 American Chemical Society. † Republished with permission of Royal Society of Chemistry, from [37] copyright 2016; permission conveyed through Copyright Clearance Center, Inc. ¥ Reprinted from [38], Copyright (2016), with permission from Elsevier.

Wang et al. [34] prepared three photocatalysts with various Ce/Ti molar ratios, 1:2, 1:1, and 2:1. All prepared CeO₂-TiO₂ composites had higher photoactivity for the CO₂ photoreduction to CH₄ and CO, when compared with Mes-CeO₂, Mes-TiO₂ and commercial TiO₂ photocatalyst (P25). This enhancement of the photocatalytic efficiency for these CeO₂-TiO₂ photocatalysts was achieved due to the ordered large specific surface area, mesoporous architecture, 2D open-pore system that facilitates the diffusion of the reactant into the bulk of photocatalyst and consequently provides fast intraparticle molecular transfer, and also due to the absorption in the visible range due to the CeO₂ species photosensitization. The heterojunction between CeO₂ and TiO₂ also contributes to the enhancement of the CeO₂-TiO₂ composites, once the photogenerated e⁻ in the TiO₂ can be transferred for the CeO₂ under the internal electric field, improving the e⁻/h⁺ separation in the TiO₂, leading to the improvement of photoactivity under irradiation [34].

The authors also confirmed by XPS analysis that the presence of CeO₂ can increase significantly the chemisorbed of oxygen species on the surface of the ordered mesoporous CeO₂-TiO₂ composites. These O species can easily trap e⁻ and produce surface O• with outstanding reduction ability. Additionally, the mixture of Ce³⁺/Ce⁴⁺ oxidation states on the CeO₂-TiO₂ surface show that the partial metal in photocatalysts is not completely oxidized, and therefore, Ce³⁺ can react with holes and avoid the recombination of photogenerated e⁻/h⁺, leading to a higher quantum effectiveness of CO₂ photoreduction [34].

Comparing the efficiency of the three different composites, no significant differences were obtained in the obtained yields of CO and CH₄ after 325 min of irradiation. The authors analyzed the stability of the composites after irradiation and concluded that these composite were stable after the photocatalytic test [34].

Abdullah et al. [35] reported a CeO₂-TiO₂ composite for the photoreduction of CO₂ into CH₃OH under Vis irradiation. They demonstrated that the methanol yield in the presence of CeO₂-TiO₂ was three times higher than that of pure TiO₂. The researchers concluded that this improvement is due to the existence of active anatase phase of titanium dioxide with a small crystalline size, and the uniform structure and smaller bandgap of the CeO₂-TiO₂ photocatalyst increased the visible light absorption and produced more e⁻/h⁺ pairs. Furthermore, the existence of both Ce³⁺ and Ce⁴⁺ oxidation states on the surface of CeO₂-TiO₂ avoided the recombination of the photogenerated e⁻/h⁺. In this case, the e⁻ are captured by the Ce⁴⁺, and these trapped electrons are moved to the adsorbed oxygen in order to produce superoxide anion radicals, while Ce³⁺ reacts with the generated h⁺, reducing the e⁻/h⁺ recombination. As can be seen in the schematic representation in Table 3, the CeO₂ has a more negative CB energy, due to the possibility of photoexcited e⁻ transference from CB of CeO₂ to CB of TiO₂, decreasing the recombination rate of the charge carriers [35].

Jiao et al. [36] prepared four CeO₂/TiO₂-*n* photocatalysts, with the weight ratio of CeO₂ to TiO₂ of *n*/100, obtaining the samples CeO₂/TiO₂-16, CeO₂/TiO₂-8, CeO₂/TiO₂-4, and CeO₂/TiO₂-2, and compared the photoactivity of the samples with the 3D ordered macroporous TiO₂ (3DOM) and the commercial TiO₂ (P25). The outcomes demonstrated that the CeO₂/TiO₂-2, CeO₂/TiO₂-4 and CeO₂/TiO₂-8 composites had higher photoactivity than the TiO₂ and P25 samples, showing that the synergetic effect of TiO₂ and CeO₂ increased the photocatalytic efficiency. The CeO₂ sample showed the lower CO production amount. The best photocatalytic performance was obtained with the sample CeO₂/TiO₂-4. However, the amount of CO decreased with the increase in the CeO₂ loading amount (>4), showing that the amounts of CeO₂ nanolayers have optimal value. The composite sample with the higher amount of CeO₂, CeO₂/TiO₂-16, showed lower performance than the 3DOM TiO₂ and P25 samples, which can be explained due to the fact that the CeO₂ sample almost did not have photocatalytic activity for this reaction condition, and this can be the possible reason for the lower photocatalytic activity of this sample. The authors proposed a type-II photocatalytic mechanism for the CO₂ photoreduction using the CeO₂/TiO₂ composite, shown in Table 3. The increase in photoactivities during the photocatalytic reduction of CO₂ under Vis irradiation is due to the synergistic effect of the

heterojunction between CeO₂ and TiO₂ and photonic crystals. They concluded that the heterojunction between CeO₂ and TiO₂ increases the charge carriers separation, and the absorption efficiency of solar irradiation can be enhanced due to the slow light effect of the 3D ordered macroporous structure and the ordered macroporous facilitates the diffusion of the reactants [36].

Zhao et al. [37] investigated the effect of the TiO₂ polymorph phases, brookite, anatase, and rutile on the CeO₂/TiO₂ composites efficiency for the photocatalytic reduction for CO₂. They prepared CeO₂/TiO₂ composite using anatase, brookite and rutile, identified as A-TiCe, B-TiCe and R-TiCe, respectively. The results showed that the higher amount of CO yield produced was achieved using the sample rutile TiO₂/CeO₂ (R-TiCe). This enhancement in CO₂ photoreduction using the rutile TiO₂/CeO₂ sample was justified due to the formation of Ti defects at the CeO₂-rutile interfaces that improves the energy-band structure of rutile, facilitating the e⁻/h⁺ pairs' separation. To go further, the authors prepared samples of rutile TiO₂/CeO₂ with different mass ratios of CeO₂/TiO₂, with CeO₂ 5.9, 12.9 and 24.3 wt.%, obtaining the samples, R-TiCe_{0.05}, R-TiCe_{0.1}, R-TiCe_{0.2}, respectively. They compared the activity of these rutile TiO₂/CeO₂ composites with the rutile TiO₂, CeO₂ and P25. The CeO₂ had the lower photocatalytic activity. The best photocatalyst for the CO₂ photoreduction was the R-TiCe_{0.1} with the yield of CO. This result can be explained once the activity of CeO₂ is markedly lower when compared with the TiO₂, suggesting that in the CeO₂/TiO₂ composites, the TiO₂ is the principal active composition, and CeO₂ acts as a promoter [37].

Wang et al. [38] synthesized CeO₂/TiO₂ samples with CeO₂ 40, 20 and 10 wt.%, identified as 0.4 CeO₂/TiO₂, 0.2 CeO₂/TiO₂ and 0.1 CeO₂/TiO₂, respectively. The activity of the CeO₂/TiO₂ composites was compared with the CeO₂ and TiO₂ samples. Comparing all the samples, the best photocatalyst was the 0.2 CeO₂/TiO₂. Furthermore, they observed that the CeO₂/TiO₂ composites' photoactivity enhances with the higher CeO₂ amount and reaches a maximum at 20 wt.% CeO₂ content (sample 0.2 CeO₂/TiO₂), since for the sample with higher CeO₂ content, the photocatalytic activity decreased. TiO₂ is the principal active composition, while CeO₂ acts as a promoter in the CeO₂/TiO₂ composites. CeO₂ content is the dominant factor on the enhancement of CO₂ photoreduction under simulated sunlight illumination. This work showed that CeO₂ extends the light absorption of the CeO₂/TiO₂ composite to the Vis range and enhances the e⁻/h⁺ separation, due to the presence of Ce³⁺ [38].

2.3. CuO/TiO₂

Copper oxide, CuO, is an p-type semiconductor nanomaterial with a bandgap between 1.2 and 1.9 eV, among this narrow direct bandgap. This material has various properties, such as high electrical conductivity, good semiconducting nature, thermal stability, low toxicity and low cost. The bandgap of CuO should favor the Vis light absorption and enhance the photoactivity [41,67,68]. CuO has been used as photocatalyst for the CO₂ photocatalytic conversion to solar fuels [69,70]. CuO exhibits spontaneous CO₂ adsorption ($\Delta H = -45 \text{ kJ mol}^{-1}$) in comparison with TiO₂. The energy levels of the CO₂-adsorbed species, such as -O-Cu-O-, can lead to an improvement in the visible-light absorption and efficient separation of electrons and holes that favors the photocatalytic activity of CuO [69,71]. Moreover, CuO presents selectivity to the formation of value-added solar fuels, such as CH₃OH and CH₄ in the photocatalytic CO₂ reduction [72]. For the above reasons, CuO/TiO₂ photocatalysts with heterojunction were also studied for the CO₂ photocatalytic reduction. CO₂ photocatalytic reduction using CuO/TiO₂ heterojunction photocatalysts is tabulated in Table 4.

Table 4. CO₂ photoreduction using CuO/TiO₂ heterojunction photocatalysts.

Photocatalysts		CO ₂ Photoreduction Condition			Yield of Products	Type of Heterojunction	Ref.
Type	Prepared	Reaction Mixture	Light Source	Conditions			
CuO/TiO ₂ (AB)	Impregnation method	pure CH ₃ OH solution (30 mL), and pure CO ₂ gas	250 W Hg lamp intensity 3900 μW/cm ² at 365 nm	ideal mixing 50 mL quartz tube Photocatalyst concentration in 1 g L ⁻¹	HCOOCH ₃ = ~1800 μmol g _{cat} ⁻¹ after 4 h	-	[41]
3 wt.% CuO/TiO ₂	Impregnation method	CO ₂ (Ultra high purity grade), 130 mL of 0.2 M KHCO ₃ and 0.1 M Na ₂ SO ₃ aqueous solutions	500 W high pressure Hg lamp with a peak light intensity at 365 nm	quartz reactor Photocatalyst concentration in 2.77 g L ⁻¹	methanol = 12.5 μmol g ⁻¹ ethanol = 27.1 μmol g ⁻¹ after 6 h	-	[42]
1.0CuO-TiO ₂	Stirring method followed by calcination	CO ₂ (99.99% purity) and 30 mL of methanol	250 W high pressure mercury lamp with the radiation peak at about 365 nm	slurry reactor system Photocatalyst concentration in 1 g L ⁻¹	Methyl formate ~1600 μmol g ⁻¹ h ⁻¹	Z-scheme * 	[39]
CuO loaded TiO ₂ nanotube	Hydrothermal method	CO ₂ (flow rate of 30 mL min ⁻¹) and ultrapure water, and NaHCO ₃ (0.1 M)	400 W high-pressure mercury lamp with a quartz filter	flow system with an inner-irradiation-type reaction vessel at ambient pressure Photocatalyst amount 0.5 g	100% CO ₂ conversion into CH ₄ and CH ₃ OH after 2.5 h	Type-I ‡ 	[43]

* Reprinted from [39], Copyright (2011), with permission from Elsevier. ‡ Reprinted from [43], Copyright (2018), with permission from Elsevier.

Zhao et al. successfully prepared CuO-incorporated TiO₂ photocatalysts by an impregnation method, to be used as photocatalysts for the CO₂ reduction into methyl formate in methanol [41]. They observed that the heterojunction photocatalyst CuO/TiO₂(AB) had higher methyl formate yield than the pristine photocatalysts. It was caused by its mixed-phase heterojunction structure and higher specific surface area, resulting in an effective separation, an enhanced UV-light response, and a smaller recombination rate of photogenerated electrons and holes. CuO/TiO₂(AB) also demonstrated sufficient stability. The methyl formate yield reproducibility was higher than 90% in cyclic runs [41]. The experimental conditions are resumed in Table 4.

Li et al. [42] dealt with CO₂ photocatalytic reduction to produce CH₃OH and C₂H₅OH over CuO-loaded titania powders suspended in H₂O with Na₂SO₃, which was the hole scavenger and promoted the formation of ethanol. The authors prepared four composites with a copper amount between 1 and 7 wt.% (7 wt.% CuO/TiO₂, 5 wt.% CuO/TiO₂, 3 wt.% CuO/TiO₂, and 1 wt.% CuO/TiO₂). They observed that yields of methanol and ethanol are enhanced with a CuO amount until 3 wt.%, and for the samples with 5 and 7 wt.%, the yields are decreased, being in this case 3 wt.%, the ideal amount of CuO loading. Loading of CuO enhances CH₃OH and C₂H₅OH yields due to the higher amount of active sites. Copper is an electron catcher and inhibits e⁻/h⁺ recombination. However, the samples with a higher amount of copper (>3 wt.% CuO) cannot further enhance the CH₃OH and C₂H₅OH yields due to the excess of CuO, which covers the surface of TiO₂, decreasing the TiO₂ photoexciting capacity, thereby reducing the photoactivity [42].

Another example of CuO and TiO₂ heterojunction was reported by Qin et al. [39]. They studied the photocatalytic reduction of carbon dioxide in CH₃OH to methyl formate in the presence of CuO–TiO₂ photocatalysts. The methanol was used as the hole scavenger, which can react with the photogenerated holes in the VB, and CO₂ was reduced by the e⁻ in the VB. The authors prepared samples with 0.5, 1, 3 and 5 weight percentage of CuO and compared their photocatalytic activity with TiO₂. The coupling of TiO₂ with CuO led to the rapid increase in the photoactivity because TiO₂ and CuO created composite photocatalysts, and electron and hole recombination was reduced.

However, as mentioned above, these authors also concluded that higher CuO loading (>1.0%, in this case) decreases the photoactivity because of the CuO particles' agglomeration. The most active photocatalyst was 1.0CuO–TiO₂ (1 wt.% of CuO). The authors concluded that the heterojunction between TiO₂ and CuO was the decisive parameter for enhancing the photoactivity of the samples [39].

Razali et al. [43] prepared p–n type CuO–TiO₂ nanotube samples with improved ability for carbon dioxide photoconversion into fuels. They concluded that the higher photocatalytic efficiency of CuO–TiO₂ photocatalyst is attributed to the restraint of e⁻ photogeneration and h⁺ recombination, as the p–n heterojunction between the CuO particles and TiO₂ nanotube facilitates the charge separation between electrons and holes, due to the presence of an electrostatic field at the junction. Electrons in the CB of CuO transfer into the CB of TiO₂, whereas holes in the VB of TiO₂ transfer to the VB of CuO. The charge transfers and separation between both semiconductors may prohibit the recombination of electrons and holes, thus increasing the photocatalytic performance of the CuO-loaded TiO₂ nanotube [43].

2.4. CdS/TiO₂

Cadmium sulfide (CdS) is a semiconductor material from the II–VI group with a direct bandgap of 2.4 eV [73,74]. CdS is used for carbon dioxide photocatalytic reduction under UV light irradiation [11,75]. This photocatalyst has ideal properties, such as the capability of converting light energy into chemical, optical, photophysical and photochemical energy [73]. However, this material has some disadvantages, such as fast e⁻/h⁺ recombination, and photocorrosion vulnerability in aqueous solution due to oxidation by photo-generated holes during photocatalytic reaction [73]. Nevertheless, the photocatalytic activity of this semiconductor can be enhanced, for instance, by doping with metal

elements or by the combination with other semiconductors [73]. To date, CdS is widely used in the TiO₂/CdS coupled heterojunction to improve the photoelectron conversion efficiency of photocatalysis and solar cell [74]. TiO₂/CdS combination is reported as the one of the most representative hybrid semiconductors, once the valence and conduction bands of the CdS are appropriately located in relation to those of TiO₂ for higher charge separation, and also CdS can absorb a main part of visible light, as it is possible to use sunlight [44,76]. CO₂ photocatalytic reduction using CdS/TiO₂ heterojunction photocatalysts is tabulated in Table 5.

Park et al. [44] reported the photocatalytic conversion of CO₂ to CH₄ in the presence of TiO₂/CdS in an isopropanol (IPA) solution under UV-Vis and Vis light irradiation. IPA is frequently used as a sacrificial e⁻ donor, such as an h⁺ scavenger. The authors prepared three TiO₂/CdS composites, TiO₂/CdS-5, TiO₂/CdS-3 and TiO₂/CdS-1, with varied amounts of loaded CdS to TiO₂, approximately 33.7%, 23.6%, and 11.4%, respectively. However, they did not observe a significant difference on the obtained yields with the CdS amount on the TiO₂, so they only reported the results obtained using the sample TiO₂/CdS-3 as a photocatalyst for the CO₂ photoreduction. The authors analyzed the H₂ evolution and the production of CO and CH₄, using Ar or CO₂ gas to purge (before irradiation) the aqueous TiO₂ and TiO₂/CdS suspensions with isopropanol.

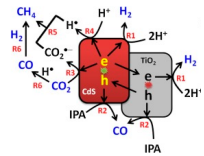
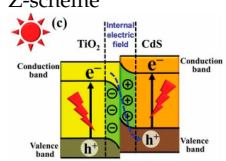
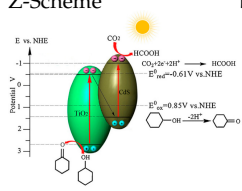
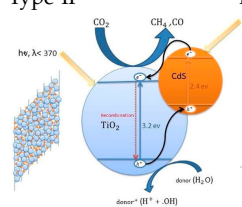
During the H₂ evolution, the results showed that using Ar-purged gas, the TiO₂/CdS composite sample had better photocatalytic activity in comparison with the pristine TiO₂. As expected, the production of H₂ in the Ar atmosphere was higher than in the CO₂ atmosphere, due to the competition for electrons. In contrast, for the CO production, it was observed that using CO₂-purged gas, the TiO₂/CdS composite sample had better photocatalytic activity in comparison with the pristine TiO₂. This result was observed due to the better adsorption of CO₂ on CdS, as well as the increased charge carrier separation and transfer on the TiO₂/CdS composite sample.

Regarding the CH₄ production, the results showed that regardless of the purge gas used (Ar or CO₂), the TiO₂/CdS composite sample had higher catalytic activity when compared with the TiO₂ sample. It is well known that CdS-modified TiO₂ is more active than pure TiO₂ for the formation of CH₄. However, in this case, some part of the CH₄ obtained was formed due to the presence of IPA, both making a contribution to the observed CH₄ yields. Furthermore, the authors did not discard the idea that the presence of hydrocarbon contaminants during the preparation of the catalyst can be considered for a fraction of the obtained yields.

The authors also investigated the photoactivity of the TiO₂/CdS sample (in CO₂-purged gas) under Vis light irradiation. In this case, only the CdS photocatalyst was capable of excitation, and no significant differences on the CH₄ production were obtained using UV-vis and visible light irradiation, suggesting that the CdS plays a significant role in CO₂ fixation and in photocatalyzing the transference of multi-electrons to CO₂.

With this work, the authors concluded that the presence of CdS on TiO₂ enhanced the production rate of CH₄ and enhanced the total CH₄ yields. They reported that this enhancement can be ascribed to the easy transference of e⁻ from the CdS to surface-bound CO₂, resulting in to the formation of •CO₂⁻ that binds to the positively charged surface of CdS, and also due to the surface-bound bicarbonate geometry that increases the production of CH₄ due to smaller energy barriers in comparison with the linear O=C=O molecule [44].

Table 5. CO₂ photoreduction using CdS/TiO₂ heterojunction photocatalysts.

Photocatalysts		CO ₂ Photoreduction Condition			Yield of Products	Type of Heterojunction	Ref.
Type	Prepared	Reaction Mixture	Light Source	Conditions			
TiO ₂ /CdS-3	Conventional hydrothermal technique	Ar or CO ₂ (both 99.99%) for 1 h, and aqueous isopropanol solution (1.0 M, 100 mL)	450 W Xe arc lamp in combination with 320 nm or 420-nm-cutoff filters	airtight glass reactor (120 mL) with a quartz disc for light penetration Photocatalyst concentration in 1 g L ⁻¹	methane = ~18 μmol (after 10 h) CO = ~2.5 μmol (after 10 h) Under UV-vis irradiation	Type-II 	* [44]
TiO ₂ /CdS	Ionic layer adsorption and reaction (SILAR) method	CO ₂ and H ₂ O vapor (from 84 mg of NaHCO ₃ and 0.3 mL of HCl solution (4 M))	300 W Xenon arc lamp	200 mL Pyrex reactor (purged with N ₂ gas) Photocatalyst: Film with 4 cm ²	11.9 mmol h ⁻¹ m ⁻² for CH ₄ production	Z-scheme 	‡ [45]
CdS-TiO ₂ -8	Hydrothermal method	CO ₂ and 10 mL cyclohexanol	250 W high pressure mercury lamp	batch slurry bed reactor with inner capacity of 50 mL Photocatalyst concentration in 2 g L ⁻¹	cyclohexyl formate = 20.2 μmol g _{cat} ⁻¹ h ⁻¹ cyclohexanone = 20 μmol g _{cat} ⁻¹ h ⁻¹	Z-Scheme 	† [46]
CdS-TiO ₂ S3 (45%)	Hydrothermal method	N ₂ and CO ₂	125 W Hg lamp (350–400 nm) For the visible light, the UV wavelengths <400 nm were removed using a sodium nitrite solution (2.0 M)	Pyrex reactor with an effective volume of 125 mL Photocatalyst concentration in 1.44 g L ⁻¹	Under UV-vis irradiation: CO = ~15.5 μmol g _{cat} ⁻¹ CH ₄ = ~3.0 μmol g _{cat} ⁻¹ after 8 h Under visible light irradiation: CO = ~10.3 μmol g _{cat} ⁻¹ CH ₄ = ~1.5 μmol g _{cat} ⁻¹ after 8 h	Type-II 	¥ [47]

* Reprinted from [44], Copyright (2016), with permission from Elsevier. ‡ Reprinted from [45], © 2022 WILEY-VCH Verlag GmbH & Co. KGaA, Weinheim. † Reprinted from [46], Copyright (2014), with permission from Elsevier. ¥ Reprinted from [47], Copyright (2014), with permission from Elsevier.

Low et al. [45] described a direct Z-scheme TiO_2/CdS composite with high efficiency for the photocatalytic reduction of CO_2 . They compared the photocatalytic activity of the TiO_2/CdS composite with the TiO_2 , CdS and commercial P25 samples. The TiO_2/CdS composite formed 3.5-, 5.4-, and 6.3-times higher amounts of CH_4 than the TiO_2 , CdS and commercial P25, respectively. They compared the type II and direct Z-scheme possibility for the mechanism of their TiO_2/CdS composites during activation. With a simple test of the $\bullet\text{OH}$ production (using coumarin to trap $\bullet\text{OH}$ and produce fluorescent products, it is possible to analyze by fluorescence spectroscopy) they concluded that it was possible to produce this radical. On the other hand, using the CdS photocatalyst was not obtained, due to the position of the VB (around 1.8 V) being lower than the potential of this reaction ($E^0(\text{OH}^-/\bullet\text{OH}) = 2.4 \text{ V}$). So, the $\bullet\text{OH}$ was formed on the TiO_2 side of the composite, following the direct Z-scheme mechanism of the charge-transfer process, as shown in the schematic illustration in Table 5. The enhanced performance obtained in the presence of the TiO_2/CdS composite can be explained due to the e^-/h^+ availability (according to the enhanced photocurrent for this sample), due to the direct Z-scheme heterojunction [45].

Song et al. [46] prepared four CdS– TiO_2 samples with various molar ratios, named CdS– TiO_2 -X (X is molar ratios of TiO_2/CdS : CdS– TiO_2 -10, CdS– TiO_2 -9, CdS– TiO_2 -8, and CdS– TiO_2 -6. All composites had higher activity for the CO_2 photoreduction than CdS and TiO_2 . This can be explained due to the interaction between TiO_2 and CdS that improved the photocatalytic reduction capacity of CO_2 .

They observed that the increase in the CdS amount in the composites until 8:1 increased the efficiency, obtaining the CdS– TiO_2 -8, optimal photoactivity for the production of cyclohexyl formate (CF) and cyclohexanone (CH). However, for CdS content higher than 8:1 TiO_2/CdS molar ratios, a decrease in the photocatalytic activity was observed, indicating that a high amount of CdS in the TiO_2 photocatalyst decreases the photogenerated e^- on the TiO_2 and then leads to a smaller photocatalytic activity. The exactly 1 mole of excited TiO_2 has to correspond to 1 mole of excited CdS; otherwise, the exceeded e^- or h^+ recombine to decrease the reaction rates. In addition, for the higher than 8:1 TiO_2/CdS molar ratios, there were difficulties in the light absorbance once the higher amount of CdS aggregated on the surface of the TiO_2 nanosheets, which hampered the absorption of light by the TiO_2 . Furthermore, they concluded that the CO_2 absorbed in cyclohexanol can be decreased to CF, and the cyclohexanol oxidized into CH on the conduction band and valence band of the TiO_2/CdS photocatalyst, respectively (as can be seen in the scheme of Table 5) [46].

Ahmad Beigi et al. [47] reported the preparation of CdS/ TiO_2 nanocomposites for the photocatalytic reduction of CO_2 to CO and CH_4 under UV-vis and visible light irradiation. For this study, four CdS/ TiO_2 samples were synthesized with different weight ratios of CdS in TiO_2 : S1 (9%), S2 (23%), S3 (45%) and S4 (74%). All CdS/ TiO_2 nanocomposites had higher photocatalytic activity than the TiO_2 and CdS samples. The CO was the majoritarian product of this reduction reaction. The presence of CdS greatly improved the photocatalytic efficiency of the TiO_2 , and the best performance was achieved using the composite CdS/ TiO_2 S3 (45%), which was the optimal ratio of CdS/ TiO_2 for CO_2 photoreduction. The enhancement used the CdS/ TiO_2 S3 (45%) composite, due to the large specific surface area and low crystal size of this sample.

As in the works reported above, the ratio of CdS in the composites was crucial to the photocatalytic performance of the composites. In this case, the authors also reported that the crystal size and specific surface area were the parameters that influenced the performance of these composites for the CO_2 reduction. Therefore, a certain amount of CdS can enhance the TiO_2 photocatalytic activity, and the porous structure of this CdS/ TiO_2 composite can have reacting sites for electrons transference to the reactant and avoid the recombination of the e^-/h^+ [47].

2.5. $\text{MoS}_2/\text{TiO}_2$

Molybdenum disulfide, MoS_2 , is a typical representative of two-dimensional (2D) transition metal chalcogenides (transition metal dichalcogenides—TMDs) [77]. Any one layer

of MoS₂ contains three atomic layers (S–Mo–S) stacked together [78]. This material is used as a substitute for noble metal co-catalysts, due to its properties, such as high activity, low cost, excellent chemical stability and abundance, and the band gap being around 1.3 to 1.9 eV [79]. Coupling TiO₂ with MoS₂ [49,80] leads to the creation of a heterojunction structure, which can speed up the electron transfer and reduce the photogenerated electrons and holes recombination. This heterojunction composite was recently studied for application on photocatalytic systems. MoS₂/TiO₂ composites were widely investigated as photocatalysts for photocatalytic degradation, hydrogen evolution, and CO₂ reduction; with this combination, the reduction of the electron/hole recombination should be possible, and also the presence of MoS₂ provides large catalytically active sites for photocatalytic progress [79]. CO₂ photocatalytic reduction using MoS₂/TiO₂ heterojunction photocatalysts is tabulated in Table 6.

Peng-yao Jia et al. in 2019 [49] synthesized the MoS₂/TiO₂ heterojunction composites with different mass ratios of MoS₂, 0, 5, 10 and 15 wt.%, obtaining the samples of TiO₂, 5 wt.% MoS₂/TiO₂, 10 wt.% MoS₂/TiO₂, and 15 wt.% MoS₂/TiO₂, respectively. The obtained results showed that the 10% MoS₂/TiO₂ sample had higher photocatalytic activity for the photoreduction of CO₂, obtaining higher amounts of CO and CH₄ than the other composite materials. The achieved yields of CH₄ and CO on the 10% MoS₂/TiO₂ heterojunction photocatalyst were approximately 5 times and 16 times higher than for pure TiO₂ (P25). This result can be explained due to the lower band gap energy of this material, and also this material showed the lowest e[−]/h⁺ recombination by PL characterization; the photocurrent characterization indicates that this sample had more enhancement in e[−] and h⁺ separation. The authors proposed a type-II heterojunction mechanism for this sample as can be seen in Table 6. Once the CB edge potential of MoS₂ (−0.93 V) is more negative than that of TiO₂ (−0.55 V), the migration of e[−] from the surface of MoS₂ to accumulate in the TiO₂ is possible, due to the contact in the interface [49].

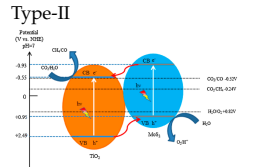

Xu et al. [50] described the preparation of 1D/2D TiO₂/MoS₂ nanostructured photocatalysts for increased photocatalytic CO₂ reduction. The authors prepared different TiO₂/MoS₂ samples, with 1%, 5%, 7.5%, 10%, 15% and 25% of MoS₂, labelled as TM_x, where T and M are TiO₂ and MoS₂, respectively, and x denotes the mol.% of MoS₂ to TiO₂.

They observed that the formation rate of CH₄ and CH₃OH was markedly increased with higher MoS₂ loading. The maximum value for the CH₄ and CH₃OH yields was reached for the TM10 sample. On the other side, only CH₃OH was observed as the product in the presence of pure TiO₂.

The authors concluded that the enhanced photocatalytic efficiency of TM10 is attributed to the increased light absorption, implying that more optical energy is absorbed after hybridization; the increased specific surface area nominates a higher amount of accessible reactive sites between TiO₂/MoS₂ and CO₂ molecules; there is a higher CO₂ adsorption capacity since CO₂ adsorption is the beginning step for the next reduction processes; and there is enhanced charge separation, owing to the presence of MoS₂ nanosheets as a cophotocatalyst [50].

In the TiO₂/MoS₂ samples, the photoinduced e[−] in TiO₂ transfers to MoS₂, reaching more efficient electron–hole separation. Thus, the number of catalytically active e[−] is significantly improved over pure TiO₂, favoring the 8 e[−] reaction for producing CH₄. For that reason, the TM_x showed higher photocatalytic CO₂ reduction activity and better selectivity of CH₄ than the pure TiO₂ photocatalyst. However, the next increasing amount of MoS₂ resulted in a decrease in the photocatalytic activity (e.g., TM25 and TM15), probably because of the severe charge carrier recombination and the shielding effects toward light absorption or the transfer of electrons, owing to the presence of a high amount of MoS₂.

Table 6. CO₂ photoreduction using MoS₂/TiO₂ heterojunction photocatalysts.

Photocatalysts		CO ₂ Photoreduction Condition			Yield of Products	Type of Heterojunction	Ref.	
Type	Prepared	Reaction Mixture	Light Source	Conditions				
10% MoS ₂ /TiO ₂	Calcined at 300 °C for 4 h with argon shielding gas	100 mL deionized H ₂ O which was preprocessed for 30 min with CO ₂ (99.99%) of 100 kPa	Xe-arc lamp 300 W acting	500 cm ³ cylindrical reactor Photocatalyst concentration in 0.5 g L ⁻¹	CO = 268.97 μmol g _{cat} ⁻¹ CH ₄ = 49.93 μmol g _{cat} ⁻¹ after 6 h	Type-II 	*	[49]
10% MoS ₂ /TiO ₂	In situ growing MoS ₂ nanosheets onto TiO ₂ nanofibers by hydrothermal method	CO ₂ and H ₂ O vapor were in situ generated by the reaction of NaHCO ₃ (0.12 g) and H ₂ SO ₄ aqueous solution (0.25 mL, 2 M)	350 W Xe lamp	200 mL homemade Pyrex reactor Photocatalyst concentration in 0.25 g L ⁻¹	CH ₄ = 2.86 μmol g ⁻¹ h ⁻¹ CH ₃ OH = 2.55 μmol g ⁻¹ h ⁻¹	Type-II 	‡	[50]
0.5 wt% MoS ₂ /TiO ₂	Hydrothermal method	200 mL of 1 M NaHCO ₃ solution and pure CO ₂	300 W Xenon arc lamp.	airtight quartz glass reactor Photocatalyst concentration in 0.5 g L ⁻¹	CH ₃ OH = 10.6 μmol g ⁻¹ h ⁻¹	-	-	[51]

* Reprinted from [49], Copyright (2019), with permission from Elsevier. ‡ Reprinted from [50], © 2022 WILEY-VCH Verlag GmbH & Co. KGaA, Weinheim.

In this study, the author also analyzed the stability of the TM10 catalyst in consecutive reutilizations and concluded that TM10 is stable without loss of photoactivity for four cycles.

Test with an isotope tracer confirmed that the products of CO₂ photocatalytic reduction solely originated from the CO₂ source. The DFT calculation demonstrated that TiO₂ has a higher work function than MoS₂, resulting in electrons transfer from MoS₂ to TiO₂ upon their contact, which supports the charge carrier separation of upon photoexcitation as MoS₂ acts as a cophotocatalyst. Moreover, the hybridization with MoS₂ increases light harvesting and enhances the CO₂ adsorption of TiO₂, further contributing to the superior photocatalytic efficiency of the TiO₂/MoS₂ hybrid [50].

Tu et al. [51] described the preparation of two-dimensional MoS₂-TiO₂ hybrid nanojunctions, for the CO₂ photocatalytic reduction to CH₃OH. They prepared MoS₂/TiO₂ photocatalysts with 3, 2, 1, and 0.5 wt.% contents of MoS₂.

All samples proved photocatalytic activity for CO₂ photoreduction into CH₃OH, the 0.5 wt.% MoS₂/TiO₂ sample being the one with the best photocatalytic performance for this reaction. Using this sample, CH₃OH production was almost three times higher than using pure TiO₂. However, for the samples with higher MoS₂ content (1, 2, and 3 wt.%) a gradual decrease in the photocatalytic activity was obtained. This occurs due to the fact that the photons in the photocatalytic system are absorbed by the excess of black MoS₂ nanosheets, and probably decrease the light intensity through shielding the light reached on the TiO₂ surface (i.e., “shielding effect”).

It was found that the two-dimensional MoS₂/TiO₂ hybrid composites presented high photocatalytic activity for CO₂ photoreduction. They concluded that loaded MoS₂ nanosheets minimize the charge carrier recombination and enhance the conversion performance of the CO₂ photoreduction into CH₃OH due to the e⁻ transfer from TiO₂ to MoS₂ [51].

2.6. Other Semiconductors

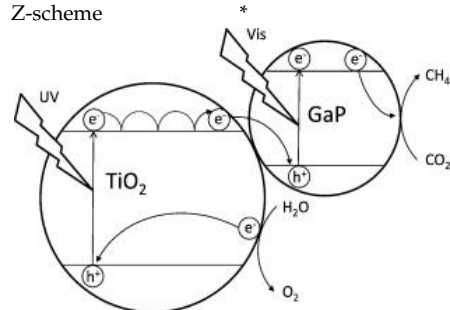
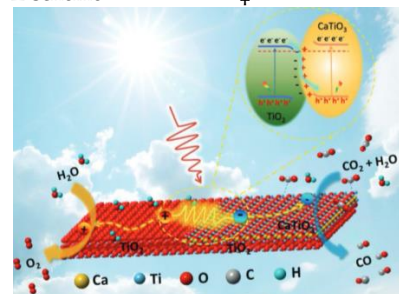
In this section, studies on the CO₂ photoreduction using composite materials with heterojunction with TiO₂ not so often used until now are shown. CO₂ photocatalytic reduction using GaP/TiO₂, CaTiO₃/TiO₂ and FeTiO₃/TiO₂ heterojunction photocatalysts are tabulated in Table 7.

2.6.1. GaP/TiO₂

Gallium phosphide, GaP, is a semiconductor material with an indirect band gap of 2.3 eV, insoluble in water. This semiconductor is not often used as a photocatalyst due to the low oxidizing power of its VB; however, the conduction band (CB) position allows the CO₂ reduction once it is 1.26 V more negative than that of CO₂/CH₄ ($E^0 = -0.24$ V) and 0.97 V more negative than CO₂/CO ($E^0 = -0.53$ V), as can be seen in the reactions from Table 1.

In 1978, Halmann [81] used GaP for the photoelectrochemical reduction of CO₂. In this case, GaP was used in the liquid junction of solar cells, and the obtained products were formic acid, formaldehyde and methanol [52,81]. Furthermore, recently, Barton et al. also used GaP and found that a highly selective CO₂ photoreduction to CH₃OH occurred when a GaP electrode with pyridine was used. In this case, pyridine served as a cocatalyst [52,82]. Regardless of the fact that electrons from the GaP conduction band can reduce CO₂ to methane, we need to look at the oxidation reaction as well. For example, often water or water vapor is chosen as the hole trap (oxidation step). In this case, water cannot be used as a hole trap because the GaP valence band ($E^0 = 0.80$ V) does not have sufficient potential for water oxidation ($E^0 = 0.82$ V). Therefore, the pristine GaP cannot be used for the CO₂ photocatalytic reduction.

Table 7. CO₂ photoreduction using GaP/TiO₂, CaTiO₃/TiO₂ and FeTiO₃/TiO₂ heterojunction photocatalysts.

Photocatalysts		CO ₂ Photoreduction Condition			Yield of Products	Type of Heterojunction	Ref.
Type	Prepared	Reaction Mixture	Light Source	Conditions			
1:10 GaP/TiO ₂	Mechanically milling of Commercial TiO ₂ Evonik P25 and GaP Aldrich powders	CO ₂ and water	1500 W high pressure Xe lamp	gas–solid Pyrex batch photoreactor of cylindrical shape (V = 100 mL, Φ = 94 mm, height = 15 mm) Photocatalyst concentration in 3 g L ⁻¹	CH ₄ = 118.18 μM g ⁻¹ after 10 h	Z-scheme 	[52]
20% FeTiO ₃ /TiO ₂	Hydrothermal method	30 mL distilled water containing sodium bicarbonate (NaHCO ₃ , 0.08 M)	500 W high-pressure Xe lamp. A Pyrex glass tube cut off light with λ < 300 nm and a 2 M NaNO ₂ solution was applied to cut off λ < 400 nm	quartz reaction vessel, connected to a gas chromatograph. Photocatalyst concentration in 1.7 g L ⁻¹	CH ₃ OH = 0.462 μmol g ⁻¹ h ⁻¹ under UV-vis irradiation and CH ₃ OH = 0.432 μmol g ⁻¹ h ⁻¹ under visible light irradiation.	-	[53]
13.4% CaTiO ₃ /TiO ₂	In situ hydrothermal method	CO ₂ and water	300 W Xe lamp	Quartz tube reactor, with 43 mL volume Photocatalyst concentration in 0.23 g L ⁻¹	CO = 11.72 μmol g ⁻¹ h ⁻¹	Z-scheme 	[54]

* Reprinted from [52], Copyright (2014), with permission from Elsevier. ‡ Republished with permission of Royal Society of Chemistry, from [54] copyright 2019; permission conveyed through Copyright Clearance Center, Inc.

In line with this, Giuseppe Marci et al. [52], for the first time, evaluated the GaP/TiO₂ composites for the photocatalytic reduction of carbon dioxide. The suitable position of VB and CB of the semiconductors not only allows for heterojunction photocatalysts (GaP/TiO₂) to have efficient electron–hole separation, but also enables both H₂O oxidation and CO₂ reduction.

Giuseppe Marci et al. [52] reported GaP/TiO₂ photocatalysts with significant efficiency during the photocatalytic reduction of carbon dioxide to the formation of methane. The researchers concluded that decreasing the mass ratio of the GaP:TiO₂ enhances the photoactivity of the photocatalyst, and the highest efficiency was observed in the presence of photocatalysts with a 1:10 mass ratio. The photocatalytic effectiveness of the photocatalysts was connected with the band structures of the semiconductors and also with the efficient electron–hole transfer between GaP and TiO₂ in the heterojunction photocatalysts.

2.6.2. FeTiO₃/TiO₂

Another interesting alternative to improve the TiO₂ photocatalytic reduction of CO₂ is the combination with ternary oxides, such as ilmenite (FeTiO₃) and perovskite (CaTiO₃); these heterojunction composite materials have not been studied very much for the photoreduction of CO₂. However, the works reported by Truong et al. [53] and Lin et al. [54] showed that FeTiO₃/TiO₂ and CaTiO₃/TiO₂, respectively, are promising materials for this photocatalytic reaction.

Ilmenite (FeTiO₃) is a semiconductor material with a band gap energy between 2.59 and 2.90 eV. This is one of the most abundant minerals used as raw material for the production of TiO₂ and Ti. FeTiO₃ has been studied by several researchers, due to its optic, semiconductive and magnetic properties, low-cost and high abundancy (as natural ilmenite), being an alternative semiconductor for photoactivated processes [83–88]. This semiconductor has been used for the formation of hetero-interfaces, with other different semiconductors, such as p–n junctions and Schottky contacts for effective carrier separation [89]. Recently, it was reported the high efficiency of FeTiO₃ as a photocatalyst for hydrogen production [83]. Furthermore, several works have been reported with the preparation and utilization of FeTiO₃-TiO₂ composites as photocatalysts for the degradation of organic pollutants, showing that this combination improves the photocatalytic activity [84,85,90,91].

Truong et al. [53] showed the photocatalytic reduction of CO₂ using the FeTiO₃/TiO₂ photocatalyst. The authors reported the preparation of a heterojunction sample of FeTiO₃/TiO₂ with various Fe/Ti mole ratios of 70%, 50%, 20%, and 10% [53]. All FeTiO₃/TiO₂ composites had a significantly higher photoactivity for the carbon dioxide reduction under both radiation sources (UV–Vis and visible light) in comparison with the TiO₂ and P25 samples. This can be explained due to the heterojunction effect between the two semiconductors, and also the higher activity in the visible light due to the combination of TiO₂ with FeTiO₃. In the FeTiO₃/TiO₂ composites, the e[−] in the valence band of TiO₂ transfer to FeTiO₃ VB, while the h⁺ are subsequently created in TiO₂ CB. Furthermore, the e[−]/h⁺ are photogenerated, owing to the narrow bandgap of FeTiO₃ [53,91]. The obtained results showed that 20% FeTiO₃/TiO₂ sample had the best photocatalytic activity. In cases with a higher amount of FeTiO₃ (50% and 70%), the CH₃OH production decreased. This was explained by the smaller surface area, and also the high metal amount in FeTiO₃/TiO₂, which can represent recombination centers, resulting in reduced photocatalytic efficiency. The enhanced photoactivity along with an increasing amount of FeTiO₃ is reasonable, due to the higher number of active sites for the carbonate species reduction. The optimal FeTiO₃ amount for the highest photocatalytic efficiency is 20 wt.%. The authors concluded with this study that the unique band structure, the heterojunction effect of two materials, and the FeTiO₃ narrow bandgap were responsible for the significant photocatalytic effectiveness on selective CH₃OH production during CO₂ photoreduction [53].

2.6.3. CaTiO₃/TiO₂

CaTiO₃ is a titanium-based perovskite-type oxide, and an n-type semiconductor with a large band gap between 3.0 and 3.5 eV. This is an alkaline earth metal titanate that is

non-toxic, with chemical stability, optical properties, a low cost and an eco-friendly nature. Currently, it is being used for several applications, such as electronic devices, photocatalytic degradation of dyes, water splitting for H₂ production and CO₂ reduction [92]. CaTiO₃ has been studied for the preparation of heterostructured photocatalysts systems to improve their photocatalytic activity, in order to promote separation and photogenerated charge carrier transportation, also leading to the improvement in their visible light response. For example, coupling CaTiO₃ with TiO₂ was studied for organic pollutants' photodegradation [93]; however, for the CO₂ reduction, only one study was reported to date.

Lin et al. [54] synthesized four CaTiO₃/TiO₂ composite samples with different amounts of TiO₂, 0.4, 0.3, 0.2 and 0.1 g, obtaining samples named 8.6%CaTiO₃/TiO₂, 13.4%CaTiO₃/TiO₂, 24.2%CaTiO₃/TiO₂ and 66.7%CaTiO₃/TiO₂, respectively, with the weight contents of CaTiO₃ obtained by XRD quantification.

The activity of these four CaTiO₃/TiO₂ had higher photoactivity for the CO₂ photoreduction than the TiO₂ and P25 samples. The best sample for this reduction reaction was 13.4%CaTiO₃/TiO₂, being that the photocatalytic activity of this sample was six times higher than the TiO₂. The results also showed that the CaTiO₃ and TiO₂ ratio influenced the photocatalytic activity efficiency for the CO₂ photoreduction, i.e., the increase in CaTiO₃ content above 13.4%CaTiO₃/TiO₂ decreased the CO evolution. The authors reported that when an excess of CaTiO₃ content was introduced, a nanocubic morphology was obtained instead of a nanosheets morphology, and also the specific surface area decreased, being the reason for the decrease in the CO production. The authors concluded that the enhancement in the CaTiO₃/TiO₂ composites catalytic activity for CO₂ photoreduction was attributed to the similar crystal structures and the matched band structures of the CaTiO₃/TiO₂ heterojunction photocatalysts that simplified the photogenerated electron–hole separation, as well as the increased surface basicity of the CaTiO₃/TiO₂ samples that provided more abundant active sites for adsorption of CO₂ and, therefore, increased the photoreduction CO₂ [54].

2.7. Semiconductor-Covalent Organic Framework Z-Scheme Heterojunctions

The integration of covalent organic frameworks (COFs) with inorganic materials gives possibilities to develop new type of composite materials [94]. These materials have high surface areas and novel functionalities relevant to photocatalysis, chemical adsorption, and magnetic resonance imaging. The disadvantages of these materials associated with challenging, multi-step synthesis were overcome by Zhu et al. [94], who reported a one-pot synthesis approach, using a wide range of metal oxides to catalyze the synthesis of highly crystalline and porous COFs.

A series of COF semiconductor Z-scheme photocatalysts integrating semiconductors (TiO₂, Bi₂WO₆ and α -Fe₂O₃) with COFs (COF-316/318) were synthesized and characterized by Zhang et al. [95]. Prepared photocatalysts showed high photocatalytic CO₂ conversion to CO efficiency, with H₂O as an electron donor in the gas–solid CO₂ reduction without additional photosensitizers and sacrificial agents. This is the first report of a covalent-bonded COF-inorganic semiconductor Z-scheme applied for artificial photosynthesis. The COF-318-TiO₂ Z-scheme heterojunction photocatalyst showed the highest CO production rate, which was about six times higher than the pure COF-318, and TiO₂ was also much higher than the physical mixture composites. Experiment studies and density functional theory (DFT) confirmed the efficient electron transfer from semiconductors to COFs by covalent coupling, resulting in the electrons being accumulated in cyano/pyridine of COF for the reduction of CO₂ and positive holes remaining in the semiconductor for the oxidation of H₂O. This work found a new method to create a covalent bond linked organic–inorganic Z-scheme heterojunction and showed a new perspective in the field of photocatalysis.

3. Final Conclusions

Nowadays, energy depletion and environmental pollution is one of the most discussed topics. The photocatalytic reduction of carbon dioxide into valuable and clean fuels can

be one of the sustainable solutions to reduce carbon dioxide emissions. Although photocatalytic CO₂ reduction has received unprecedented attention from scientists worldwide, its widespread use is limited due to the low selectivity, stability and especially the low efficiency of the photocatalytic system. The most studied photocatalyst in recent years is TiO₂ because it is cheap, non-toxic and environmentally friendly. Unfortunately, TiO₂ has some limitations, such as its activation, especially in the UV region, or the rapid recombination of generated electrons and holes. These imperfections can be tuned by doping TiO₂ with metals or non-metals or by creating TiO₂ heterojunction photocatalysts with other semiconductors.

In this review, TiO₂ heterojunction photocatalysts were discussed to further increase the photocatalytic efficiency of TiO₂ photocatalysts. In the last few years, several studies have been published on the preparation of TiO₂ heterojunction photocatalysts suitable for photocatalytic CO₂ reduction. Using these materials with the heterojunction, it was possible to improve the catalytic activity for the photoreduction of CO₂, due to the efficient electron transference in the interface, supporting the separation of the e⁻/h⁺ pairs and consequently reducing the e⁻/h⁺ recombination. In addition, the activity in the visible light range was improved because it was possible to utilize sunlight more effectively; there was higher adsorption of CO₂ due to the highly specific surface area; and there was an increase in selectivity specific CO₂ photoreduction products due to the contribution of the cocatalysts. In the case of heterojunction photocatalysts, there is always an optimal amount or ratio of semiconductors used. The use of the metal as a dopant TiO₂, which then forms a heterojunction with C₃N₄, also proved to be very advantageous.

Further research in this area should focus on the following aspects:

- To create heterojunction photocatalysts, it is essential to find materials that have the appropriate band structure for redox reactions, are active in the visible light region, and are stable.
- Efforts are underway to develop not too complex, efficient and effective methods for preparing heterojunction photocatalysts that could be produced in larger quantities. The most appropriate physicochemical properties of each semiconductor, such as the appropriate morphology, crystallite size, phase composition, etc., should be considered when developing preparation methods.
- The migration pathways of photogenerated electron–hole pairs need to be thoroughly studied. Heterojunction photocatalysts can have different arrangements (e.g., heterojunction type II or Z-scheme heterojunction) and, thus, different migration pathways for electron–hole separation, which need to be thoroughly studied and confirmed using advanced characterization techniques.
- To better understand the mechanism of migration pathways, knowledge from modeling methods or theoretical calculations should be used.

We hope that this review will encourage new approaches to the preparation of heterojunction photocatalysts, help optimize existing photocatalysts and create new efficient heterojunctions to achieve the higher efficiencies that are necessary for practical applications.

Author Contributions: Conceptualization, B.T.B., N.A. and K.K.; methodology, B.T.B., N.A. and K.K.; investigation, B.T.B., N.A. and K.K.; writing—original draft preparation, B.T.B., N.A. and K.K.; writing—review and editing, B.T.B. and K.K.; supervision, K.K. All authors have read and agreed to the published version of the manuscript.

Funding: This research was funded by Scientific Science Foundation of the Czech Republic (No. 20-09914S), by EU structural funding in Operational Programme Research, Development and Education, project No. CZ.02.1.01./0.0/0.0/17_049/0008419 “COOPERATION”.

Conflicts of Interest: The authors declare no conflict of interest.

References

1. Hannah, R.; Roser, M. CO₂ and greenhouse gas emissions. Our World Data 2017. Available online: <https://ourworldindata.org/co2-and-other-greenhouse-gas-emissions> (accessed on 15 October 2021).
2. Lee, C.W.; Yang, K.D.; Nam, D.-H.; Jang, J.H.; Cho, N.H.; Im, S.W.; Nam, K.T. Defining a materials database for the design of copper binary alloy catalysts for electrochemical CO₂ conversion. *Adv. Mater.* **2018**, *30*, 1704717. [[CrossRef](#)] [[PubMed](#)]
3. Appel, A.M.; Bercaw, J.E.; Bocarsly, A.B.; Dobbek, H.; DuBois, D.L.; Dupuis, M.; Ferry, J.G.; Fujita, E.; Hille, R.; Kenis, P.J.A.; et al. Frontiers, Opportunities, and challenges in biochemical and chemical catalysis of CO₂ fixation. *Chem. Rev.* **2013**, *113*, 6621–6658. [[CrossRef](#)]
4. Kočí, K.; Dang Van, H.; Edelmannová, M.; Reli, M.; Wu, J.C.S. Photocatalytic reduction of CO₂ using Pt/C₃N₄ photocatalysts. *Appl. Surf. Sci.* **2020**, *503*, 144426. [[CrossRef](#)]
5. Habisreutinger, S.N.; Schmidt-Mende, L.; Stolarczyk, J.K. Photocatalytic reduction of CO₂ on TiO₂ and other semiconductors. *Angew. Chem. Int. Ed.* **2013**, *52*, 7372–7408. [[CrossRef](#)] [[PubMed](#)]
6. Hiragond, C.; Ali, S.; Sorcar, S.; In, S.-I. Hierarchical nanostructured photocatalysts for CO₂ photoreduction. *Catalysts* **2019**, *9*, 370. [[CrossRef](#)]
7. Ziarati, A.; Badiie, A.; Grillo, R.; Burgi, T. 3D Yolk@Shell TiO_{2-x}/LDH architecture: Tailored structure for visible light CO₂ conversion. *ACS Appl. Mater. Interfaces* **2019**, *11*, 5903–5910. [[CrossRef](#)]
8. Nguyen, T.P.; Nguyen, D.L.T.; Nguyen, V.-H.; Le, T.-H.; Vo, D.-V.N.; Trinh, Q.T.; Bae, S.-R.; Chae, S.Y.; Kim, S.Y.; Le, Q.V. Recent advances in TiO₂-based photocatalysts for reduction of CO₂ to fuels. *Nanomaterials* **2020**, *10*, 337. [[CrossRef](#)]
9. Gao, Y.; Qian, K.; Xu, B.; Li, Z.; Zheng, J.; Zhao, S.; Ding, F.; Sun, Y.; Xu, Z. Recent advances in visible-light-driven conversion of CO₂ by photocatalysts into fuels or value-added chemicals. *Carbon Resour. Convers.* **2020**, *3*, 46–59. [[CrossRef](#)]
10. Li, K.; Teng, C.; Wang, S.; Min, Q. Recent advances in TiO₂-based heterojunctions for photocatalytic CO₂ reduction with water oxidation: A Review. *Front. Chem.* **2021**, *9*, 637501. [[CrossRef](#)]
11. Inoue, T.; Fujishima, A.; Konishi, S.; Honda, K. Photoelectrocatalytic reduction of carbon dioxide in aqueous suspensions of semiconductor powders. *Nature* **1979**, *277*, 637–638. [[CrossRef](#)]
12. Wei, L.; Yu, C.; Zhang, Q.; Liu, H.; Wang, Y. TiO₂-based heterojunction photocatalysts for photocatalytic reduction of CO₂ into solar fuels. *J. Mater. Chem.* **2018**, *6*, 22411–22436. [[CrossRef](#)]
13. Ohtani, B.; Handa, J.-i.; Nishimoto, S.-i.; Kagiya, T. Highly active semiconductor photocatalyst: Extra-fine crystallite of brookite TiO₂ for redox reaction in aqueous propan-2-ol and/or silver sulfate solution. *Chem. Phys. Lett.* **1985**, *120*, 292–294. [[CrossRef](#)]
14. Li, Y.; Zhou, M.; Cheng, B.; Shao, Y. Recent advances in g-C₃N₄-based heterojunction photocatalysts. *J. Mater. Sci. Technol.* **2020**, *56*, 1–17. [[CrossRef](#)]
15. Liu, X.; Dang, R.; Dong, W.; Huang, X.; Tang, J.; Gao, H.; Wang, G. A sandwich-like heterostructure of TiO₂ nanosheets with MIL-100(Fe): A platform for efficient visible-light-driven photocatalysis. *Appl. Catal. B* **2017**, *209*, 506–513. [[CrossRef](#)]
16. Xiong, Z.; Wang, H.; Xu, N.; Li, H.; Fang, B.; Zhao, Y.; Zhang, J.; Zheng, C. Photocatalytic reduction of CO₂ on Pt²⁺-Pt⁰/TiO₂ nanoparticles under UV/Vis light irradiation: A combination of Pt²⁺ doping and Pt nanoparticles deposition. *Int. J. Hydrogen Energy* **2015**, *40*, 10049–10062. [[CrossRef](#)]
17. Liu, X.; Dong, G.; Li, S.; Lu, G.; Bi, Y. Direct observation of charge separation on anatase TiO₂ crystals with selectively etched {001} facets. *J. Am. Chem. Soc.* **2016**, *138*, 2917–2920. [[CrossRef](#)]
18. Low, J.; Yu, J.; Jaroniec, M.; Wageh, S.; Al-Ghamdi, A.A. Heterojunction photocatalysts. *Adv. Mater.* **2017**, *29*, 1601694. [[CrossRef](#)]
19. Low, J.; Yu, J.; Jiang, C. Design and fabrication of direct Z-scheme photocatalysts. In *Interface Science and Technology*; Yu, J., Jaroniec, M., Jiang, C., Eds.; Elsevier: Amsterdam, The Netherlands, 2020; Volume 31, pp. 193–229.
20. Bard, A.J. Photoelectrochemistry and heterogeneous photo-catalysis at semiconductors. *J. Photochem. Photobiol.* **1979**, *10*, 59–75. [[CrossRef](#)]
21. Tada, H.; Mitsui, T.; Kiyonaga, T.; Akita, T.; Tanaka, K. All-solid-state Z-scheme in CdS-Au-TiO₂ three-component nanojunction system. *Nat. Mater.* **2006**, *5*, 782–786. [[CrossRef](#)]
22. Yu, J.; Wang, S.; Low, J.; Xiao, W. Enhanced photocatalytic performance of direct Z-scheme g-C₃N₄-TiO₂ photocatalysts for the decomposition of formaldehyde in air. *Phys. Chem. Chem. Phys.* **2013**, *15*, 16883–16890. [[CrossRef](#)]
23. Yang, C.; Qin, J.; Xue, Z.; Ma, M.; Zhang, X.; Liu, R. Rational design of carbon-doped TiO₂ modified g-C₃N₄ via in-situ heat treatment for drastically improved photocatalytic hydrogen with excellent photostability. *Nano Energy* **2017**, *41*, 1–9. [[CrossRef](#)]
24. Lu, N.; Wang, C.; Sun, B.; Gao, Z.; Su, Y. Fabrication of TiO₂-doped single layer graphitic-C₃N₄ and its visible-light photocatalytic activity. *Sep. Purif. Technol.* **2017**, *186*, 226–232. [[CrossRef](#)]
25. Shi, H.; Long, S.; Hu, S.; Hou, J.; Ni, W.; Song, C.; Li, K.; Gurzadyan, G.G.; Guo, X. Interfacial charge transfer in 0D/2D defect-rich heterostructures for efficient solar-driven CO₂ reduction. *Appl. Catal. B* **2019**, *245*, 760–769. [[CrossRef](#)]
26. Reli, M.; Huo, P.; Šihor, M.; Ambrožová, N.; Troppová, I.; Matějová, L.; Lang, J.; Svoboda, L.; Kušrowski, P.; Ritz, M.; et al. Novel TiO₂/C₃N₄ photocatalysts for photocatalytic reduction of CO₂ and for photocatalytic decomposition of N₂O. *J. Phys. Chem. A* **2016**, *120*, 8564–8573. [[CrossRef](#)]
27. Zhang, L.; Xie, C.; Jiu, H.; Meng, Y.; Zhang, Q.; Gao, Y. Synthesized hollow TiO₂@g-C₃N₄ composites for carbon dioxide reduction under visible light. *Catal. Lett.* **2018**, *148*, 2812–2821. [[CrossRef](#)]
28. Banitalebi Dehkordi, A.; Ziarati, A.; Ghasemi, J.B.; Badiie, A. Preparation of hierarchical g-C₃N₄@TiO₂ hollow spheres for enhanced visible-light induced catalytic CO₂ reduction. *Sol. Energy* **2020**, *205*, 465–473. [[CrossRef](#)]

29. Zhou, S.; Liu, Y.; Li, J.; Wang, Y.; Jiang, G.; Zhao, Z.; Wang, D.; Duan, A.; Liu, J.; Wei, Y. Facile in situ synthesis of graphitic carbon nitride (g-C₃N₄)-N-TiO₂ heterojunction as an efficient photocatalyst for the selective photoreduction of CO₂ to CO. *Appl. Catal. B* **2014**, *158–159*, 20–29. [[CrossRef](#)]
30. Thanh Truc, N.T.; Giang Bach, L.; Thi Hanh, N.; Pham, T.-D.; Thi Phuong Le Chi, N.; Tran, D.T.; Nguyen, M.V.; Nguyen, V.N. The superior photocatalytic activity of Nb doped TiO₂/g-C₃N₄ direct Z-scheme system for efficient conversion of CO₂ into valuable fuels. *J. Colloid Interface Sci.* **2019**, *540*, 1–8. [[CrossRef](#)]
31. Li, H.; Gao, Y.; Wu, X.; Lee, P.-H.; Shih, K. Fabrication of heterostructured g-C₃N₄/Ag-TiO₂ hybrid photocatalyst with enhanced performance in photocatalytic conversion of CO₂ under simulated sunlight irradiation. *Appl. Surf. Sci.* **2017**, *402*, 198–207. [[CrossRef](#)]
32. Liu, C.; Raziq, F.; Li, Z.; Qu, Y.; Zada, A.; Jing, L. Synthesis of TiO₂/g-C₃N₄ nanocomposites with phosphate–oxygen functional bridges for improved photocatalytic activity. *Chin. J. Catal.* **2017**, *38*, 1072–1078. [[CrossRef](#)]
33. Sun, R.; Jiang, X.; Zhang, M.; Ma, Y.; Jiang, X.; Liu, Z.; Wang, Y.; Yang, J.; Xie, M.; Han, W. Dual quantum dots decorated TiO₂ nanorod arrays for efficient CO₂ reduction. *J. Catal.* **2019**, *378*, 192–200. [[CrossRef](#)]
34. Wang, Y.; Li, B.; Zhang, C.; Cui, L.; Kang, S.; Li, X.; Zhou, L. Ordered mesoporous CeO₂-TiO₂ composites: Highly efficient photocatalysts for the reduction of CO₂ with H₂O under simulated solar irradiation. *Appl. Catal. B* **2013**, *130–131*, 277–284. [[CrossRef](#)]
35. Abdullah, H.; Khan, M.R.; Pudukudy, M.; Yaakob, Z.; Ismail, N.A. CeO₂-TiO₂ as a visible light active catalyst for the photoreduction of CO₂ to methanol. *J. Rare Earths* **2015**, *33*, 1155–1161. [[CrossRef](#)]
36. Jiao, J.; Wei, Y.; Zhao, Z.; Liu, J.; Li, J.; Duan, A.; Jiang, G. Photocatalysts of 3D Ordered Macroporous TiO₂-Supported CeO₂ nanolayers: Design, Preparation, and their catalytic performances for the reduction of CO₂ with H₂O under simulated solar irradiation. *Ind. Eng. Chem. Res.* **2014**, *53*, 17345–17354. [[CrossRef](#)]
37. Zhao, J.; Wang, Y.; Li, Y.; Yue, X.; Wang, C. Phase-dependent enhancement for CO₂ photocatalytic reduction over CeO₂/TiO₂ catalysts. *Catal. Sci. Technol.* **2016**, *6*, 7967–7975. [[CrossRef](#)]
38. Wang, Y.; Zhao, J.; Wang, T.; Li, Y.; Li, X.; Yin, J.; Wang, C. CO₂ photoreduction with H₂O vapor on highly dispersed CeO₂/TiO₂ catalysts: Surface species and their reactivity. *J. Catal.* **2016**, *337*, 293–302. [[CrossRef](#)]
39. Qin, S.; Xin, F.; Liu, Y.; Yin, X.; Ma, W. Photocatalytic reduction of CO₂ in methanol to methyl formate over CuO–TiO₂ composite catalysts. *J. Colloid Interface Sci.* **2011**, *356*, 257–261. [[CrossRef](#)]
40. Méndez-Medrano, M.G.; Kowalska, E.; Lehoux, A.; Herissan, A.; Ohtani, B.; Bahena, D.; Briois, V.; Colbeau-Justin, C.; Rodríguez-López, J.L.; Remita, H. Surface modification of TiO₂ with Ag nanoparticles and CuO nanoclusters for application in photocatalysis. *J. Phys. Chem. C* **2016**, *120*, 5143–5154. [[CrossRef](#)]
41. Zhao, Y.; Chen, J.; Cai, W.; Bu, Y.; Huang, Q.; Tao, T.; Lu, J. CuO-decorated dual-phase TiO₂ microspheres with enhanced activity for photocatalytic CO₂ reduction in liquid–solid regime. *Chem. Phys. Lett.* **2019**, *725*, 66–74. [[CrossRef](#)]
42. Li, H.; Li, C.; Han, L.; Li, C.; Zhang, S. Photocatalytic reduction of CO₂ with H₂O on CuO/TiO₂ catalysts. *Energy Sources A Recovery Util. Environ. Eff.* **2016**, *38*, 420–426. [[CrossRef](#)]
43. Razali, M.H.; Yusoff, M. Highly efficient CuO loaded TiO₂ nanotube photocatalyst for CO₂ photoconversion. *Mater. Lett.* **2018**, *221*, 168–171. [[CrossRef](#)]
44. Park, H.; Ou, H.-H.; Kang, U.; Choi, J.; Hoffmann, M.R. Photocatalytic conversion of carbon dioxide to methane on TiO₂/CdS in aqueous isopropanol solution. *Catal. Today* **2016**, *266*, 153–159. [[CrossRef](#)]
45. Low, J.; Dai, B.; Tong, T.; Jiang, C.; Yu, J. In situ irradiated X-ray photoelectron spectroscopy investigation on a direct Z-Scheme TiO₂/CdS composite film photocatalyst. *Adv. Mater.* **2019**, *31*, 1802981. [[CrossRef](#)] [[PubMed](#)]
46. Song, G.; Xin, F.; Chen, J.; Yin, X. Photocatalytic reduction of CO₂ in cyclohexanol on CdS–TiO₂ heterostructured photocatalyst. *Appl. Catal. A* **2014**, *473*, 90–95. [[CrossRef](#)]
47. Ahmad Beigi, A.; Fatemi, S.; Salehi, Z. Synthesis of nanocomposite CdS/TiO₂ and investigation of its photocatalytic activity for CO₂ reduction to CO and CH₄ under visible light irradiation. *J. CO₂ Util.* **2014**, *7*, 23–29. [[CrossRef](#)]
48. Khalilzadeh, A.; Shariati, A. Photoreduction of CO₂ over heterogeneous modified TiO₂ nanoparticles under visible light irradiation: Synthesis, process and kinetic study. *Sol. Energy* **2018**, *164*, 251–261. [[CrossRef](#)]
49. Jia, P.-y.; Guo, R.-t.; Pan, W.-g.; Huang, C.-y.; Tang, J.-y.; Liu, X.-y.; Qin, H.; Xu, Q.-y. The MoS₂/TiO₂ heterojunction composites with enhanced activity for CO₂ photocatalytic reduction under visible light irradiation. *Colloids Surf. A Physicochem. Eng. Asp.* **2019**, *570*, 306–316. [[CrossRef](#)]
50. Xu, F.Y.; Zhu, B.C.; Cheng, B.; Yu, J.G.; Xu, J.S. 1D/2D TiO₂/MoS₂ hybrid nanostructures for enhanced photocatalytic CO₂ reduction. *Adv. Opt. Mater.* **2018**, *6*, 1800911. [[CrossRef](#)]
51. Tu, W.; Li, Y.; Kuai, L.; Zhou, Y.; Xu, Q.; Li, H.; Wang, X.; Xiao, M.; Zou, Z. Construction of unique two-dimensional MoS₂-TiO₂ hybrid nanojunctions: MoS₂ as a promising cost-effective cocatalyst toward improved photocatalytic reduction of CO₂ to methanol. *Nanoscale* **2017**, *9*, 9065–9070. [[CrossRef](#)]
52. Marci, G.; Garcia-Lopez, E.I.; Palmisano, L. Photocatalytic CO₂ reduction in gas-solid regime in the presence of H₂O by using GaP/TiO₂ composite as photocatalyst under simulated solar light. *Catal. Commun.* **2014**, *53*, 38–41. [[CrossRef](#)]
53. Truong, Q.D.; Liu, J.-Y.; Chung, C.-C.; Ling, Y.-C. Photocatalytic reduction of CO₂ on FeTiO₃/TiO₂ photocatalyst. *Catal. Commun.* **2012**, *19*, 85–89. [[CrossRef](#)]

54. Lin, J.; Hu, J.; Qiu, C.; Huang, H.; Chen, L.; Xie, Y.; Zhang, Z.; Lin, H.; Wang, X. In situ hydrothermal etching fabrication of CaTiO₃ on TiO₂ nanosheets with heterojunction effects to enhance CO₂ adsorption and photocatalytic reduction. *Catal. Sci. Technol.* **2019**, *9*, 336–346. [[CrossRef](#)]
55. Yin, S.; Han, J.; Zhou, T.; Xu, R. Recent progress in g-C₃N₄ based low cost photocatalytic system: Activity enhancement and emerging applications. *Catal. Sci. Technol.* **2015**, *5*, 5048–5061. [[CrossRef](#)]
56. Raizada, P.; Kumar, A.; Hasija, V.; Singh, P.; Thakur, V.K.; Khan, A.A.P. An overview of converting reductive photocatalyst into all solid-state and direct Z-scheme system for water splitting and CO₂ reduction. *J. Ind. Eng. Chem.* **2021**, *93*, 1–27. [[CrossRef](#)]
57. Jourshabani, M.; Shariatnia, Z.; Badiie, A. Sulfur-doped mesoporous carbon nitride decorated with Cu particles for efficient photocatalytic degradation under visible-light irradiation. *J. Phys. Chem. C* **2017**, *121*, 19239–19253. [[CrossRef](#)]
58. Jiang, Z.; Wan, W.; Li, H.; Yuan, S.; Zhao, H.; Wong, P.K. A hierarchical Z-Scheme α -Fe₂O₃/g-C₃N₄ hybrid for enhanced photocatalytic CO₂ reduction. *Adv. Mater.* **2018**, *30*, 1706108. [[CrossRef](#)]
59. Ong, W.-J.; Tan, L.-L.; Ng, Y.H.; Yong, S.-T.; Chai, S.-P. Graphitic carbon nitride (g-C₃N₄)-based photocatalysts for artificial photosynthesis and environmental remediation: Are we a step closer to achieving sustainability? *Chem. Rev.* **2016**, *116*, 7159–7329. [[CrossRef](#)]
60. Zhao, Y.; Lin, Y.; Wang, G.; Jiang, Z.; Zhang, R.; Zhu, C. Electronic and optical performances of (Cu, N) codoped TiO₂/g-C₃N₄ heterostructure photocatalyst: A spin-polarized DFT + U study. *Sol. Energy* **2018**, *162*, 306–316. [[CrossRef](#)]
61. Chen, Y.; Huang, W.; He, D.; Situ, Y.; Huang, H. Construction of Heterostructured g-C₃N₄/Ag/TiO₂ Microspheres with Enhanced Photocatalysis Performance under Visible-Light Irradiation. *ACS Appl. Mater. Interfaces* **2014**, *6*, 14405–14414. [[CrossRef](#)]
62. Jiang, G.; Cao, J.; Chen, M.; Zhang, X.; Dong, F. Photocatalytic NO oxidation on N-doped TiO₂/g-C₃N₄ heterojunction: Enhanced efficiency, mechanism and reaction pathway. *Appl. Surf. Sci.* **2018**, *458*, 77–85. [[CrossRef](#)]
63. Liu, R.; Bie, Y.; Qiao, Y.; Liu, T.; Song, Y. Design of g-C₃N₄/TiO₂ nanotubes heterojunction for enhanced organic pollutants degradation in waste water. *Mater. Lett.* **2019**, *251*, 126–130. [[CrossRef](#)]
64. Das, A.; Patra, M.; Kumar, P.M.; Bhagavathiachari, M.; Nair, R.G. Defect-induced visible-light-driven photocatalytic and photoelectrochemical performance of ZnO–CeO₂ nanoheterojunctions. *J. Alloys Compd.* **2021**, *858*, 157730. [[CrossRef](#)]
65. Islam, M.J.; Reddy, D.A.; Choi, J.; Kim, T.K. Surface oxygen vacancy assisted electron transfer and shuttling for enhanced photocatalytic activity of a Z-scheme CeO₂-AgI nanocomposite. *RSC Adv.* **2016**, *6*, 19341–19350. [[CrossRef](#)]
66. Basha, M.H.; Ramu, C.; Gopal, N.O.; Reddy, M.V.B. Structural and spectroscopic characterizations of boron doped TiO₂-CeO₂ nanocomposite synthesized by solution combustion technique for photocatalytic applications. *J. Mol. Struct.* **2021**, *1231*, 129892. [[CrossRef](#)]
67. Patil, P.; Nakate, U.T.; Nakate, Y.T.; Ambare, R.C. Acetaldehyde sensing properties using ultrafine CuO nanoparticles. *Mater. Sci. Semicond. Process.* **2019**, *101*, 76–81. [[CrossRef](#)]
68. Zhang, H.; Wang, K.; Wang, L.; Xie, H.; Yu, W. Mesoporous CuO with full spectrum absorption for photothermal conversion in direct absorption solar collectors. *Sol. Energy* **2020**, *201*, 628–637. [[CrossRef](#)]
69. Avila-Lopez, M.A.; Luevano-Hipolito, E.; Torres-Martinez, L.M. CuO coatings on glass fibers: A hybrid material for CO₂ adsorption and photocatalytic reduction to solar fuels. *J. Mater. Sci.—Mater. Electron.* **2021**, *32*, 11336–11337. [[CrossRef](#)]
70. Avila-Lopez, M.A.; Luevano-Hipolito, E.; Torres-Martinez, L.M. CO₂ adsorption and its visible-light-driven reduction using CuO synthesized by an eco-friendly sonochemical method. *J. Photochem. Photobiol. A—Chem.* **2019**, *382*, 10. [[CrossRef](#)]
71. Yan, Y.; Yu, Y.; Cao, C.; Huang, S.; Yang, Y.; Yang, X.; Cao, Y. Enhanced photocatalytic activity of TiO₂-Cu/C with regulation and matching of energy levels by carbon and copper for photoreduction of CO₂ into CH₄. *CrystEngComm* **2016**, *18*, 2956–2964. [[CrossRef](#)]
72. Nogueira, A.E.; Oliveira, J.A.; da Silva, G.T.S.T.; Ribeiro, C. Insights into the role of CuO in the CO₂ photoreduction process. *Sci. Rep.* **2019**, *9*, 1316. [[CrossRef](#)]
73. Wang, Q.; Lian, J.; Ma, Q.; Zhang, S.; He, J.; Zhong, J.; Li, J.; Huang, H.; Su, B. Preparation of carbon spheres supported CdS photocatalyst for enhancement its photocatalytic H₂ evolution. *Catal. Today* **2017**, *281*, 662–668. [[CrossRef](#)]
74. Meng, H.L.; Cui, C.; Shen, H.L.; Liang, D.Y.; Xue, Y.Z.; Li, P.G.; Tang, W.H. Synthesis and photocatalytic activity of TiO₂@CdS and CdS@TiO₂ double-shelled hollow spheres. *J. Alloys Compd.* **2012**, *527*, 30–35. [[CrossRef](#)]
75. Li, X.; Chen, J.; Li, H.; Li, J.; Xu, Y.; Liu, Y.; Zhou, J. Photoreduction of CO₂ to methanol over Bi₂S₃/CdS photocatalyst under visible light irradiation. *J. Nat. Gas Chem.* **2011**, *20*, 413–417. [[CrossRef](#)]
76. Jang, J.S.; Park, H. Strategic Design of Heterojunction CdS Photocatalysts for Solar Hydrogen. In *Materials and Processes for Solar Fuel Production*; Viswanathan, B., Subramanian, V., Lee, J.S., Eds.; Springer: New York, NY, USA, 2014; pp. 1–22.
77. Tan, C.; Zhang, H. Two-dimensional transition metal dichalcogenide nanosheet-based composites. *Chem. Soc. Rev.* **2015**, *44*, 2713–2731. [[CrossRef](#)] [[PubMed](#)]
78. Xiang, Q.; Yu, J.; Jaroniec, M. Synergetic effect of MoS₂ and graphene as cocatalysts for enhanced photocatalytic H₂ production activity of TiO₂ nanoparticles. *J. Am. Chem. Soc.* **2012**, *134*, 6575–6578. [[CrossRef](#)] [[PubMed](#)]
79. Chen, B.; Meng, Y.; Sha, J.; Zhong, C.; Hu, W.; Zhao, N. Preparation of MoS₂/TiO₂ based nanocomposites for photocatalysis and rechargeable batteries: Progress, challenges, and perspective. *Nanoscale* **2018**, *10*, 34–68. [[CrossRef](#)] [[PubMed](#)]
80. Zhou, W.; Yin, Z.; Du, Y.; Huang, X.; Zeng, Z.; Fan, Z.; Liu, H.; Wang, J.; Zhang, H. Synthesis of few-layer MoS₂ nanosheet-coated TiO₂ nanobelt heterostructures for enhanced photocatalytic activities. *Small* **2013**, *9*, 140–147. [[CrossRef](#)]

81. Halmann, M. Photoelectrochemical reduction of aqueous carbon dioxide on p-type gallium phosphide in liquid junction solar cells. *Nature* **1978**, *275*, 115–116. [[CrossRef](#)]
82. Barton, E.E.; Rampulla, D.M.; Bocarsly, A.B. Selective Solar-Driven Reduction of CO₂ to Methanol Using a Catalyzed p-GaP Based Photoelectrochemical Cell. *J. Am. Chem. Soc.* **2008**, *130*, 6342–6344. [[CrossRef](#)]
83. Cañas-Martínez, D.M.; Cipagauta-Díaz, S.; Manrique, M.; Gómez, R.; Pedraza-Avella, J.A. Photocatalytic hydrogen production using FeTiO₃ concentrates modified by high energy ball milling and the presence of Mg precursors. *Top. Catal.* **2021**, *64*, 2–16. [[CrossRef](#)]
84. Cañas-Martínez, D.M.; Gauthier, G.H.; Pedraza-Avella, J.A. Photo-oxidative and photo-reductive capabilities of ilmenite-rich black sand concentrates using methyl orange as a probe molecule. *Photochem. Photobiol. Sci.* **2019**, *18*, 912–919. [[CrossRef](#)] [[PubMed](#)]
85. Moradi, M.; Vasseghian, Y.; Khataee, A.; Harati, M.; Arfaeina, H. Ultrasound-assisted synthesis of FeTiO₃/GO nanocomposite for photocatalytic degradation of phenol under visible light irradiation. *Sep. Purif. Technol.* **2021**, *261*, 118274. [[CrossRef](#)]
86. Xiao, W.; Lu, X.-g.; Zou, X.-l.; Wei, X.-m.; Ding, W.-z. Phase transitions, micro-morphology and its oxidation mechanism in oxidation of ilmenite (FeTiO₃) powder. *Trans. Nonferrous Met. Soc. China* **2013**, *23*, 2439–2445. [[CrossRef](#)]
87. Baysal, Z.; Kirchner, J.; Mehne, M.; Kureti, S. Study on the reduction of ilmenite-type FeTiO₃ by H₂. *Int. J. Hydrogen Energy* **2021**, *46*, 4447–4459. [[CrossRef](#)]
88. García-Muñoz, P.; Pliego, G.; Zazo, J.A.; Bahamonde, A.; Casas, J.A. Ilmenite (FeTiO₃) as low cost catalyst for advanced oxidation processes. *J. Environ. Chem. Eng.* **2016**, *4*, 542–548. [[CrossRef](#)]
89. Gao, B.; Yang, C.; Chen, J.; Ma, Y.; Xie, J.; Zhang, H.; Wei, L.; Li, Q.; Du, J.; Xu, Q. Ferromagnetic photocatalysts of FeTiO₃-Fe₂O₃ nanocomposites. *RSC Adv.* **2017**, *7*, 54594–54602. [[CrossRef](#)]
90. Zarazúa-Morín, M.E.; Torres-Martínez, L.M.; Moctezuma, E.; Juárez-Ramírez, I.; Zermeño, B.B. Synthesis, characterization, and catalytic activity of FeTiO₃/TiO₂ for photodegradation of organic pollutants with visible light. *Res. Chem. Intermed.* **2016**, *42*, 1029–1043. [[CrossRef](#)]
91. Gao, B.; Kim, Y.J.; Chakraborty, A.K.; Lee, W.I. Efficient decomposition of organic compounds with FeTiO₃/TiO₂ heterojunction under visible light irradiation. *Appl. Catal. B* **2008**, *83*, 202–207. [[CrossRef](#)]
92. Passi, M.; Pal, B. A review on CaTiO₃ photocatalyst: Activity enhancement methods and photocatalytic applications. *Powder Technol.* **2021**, *388*, 274–304. [[CrossRef](#)]
93. Cesconeto, F.R.; Borlaf, M.; Nieto, M.I.; de Oliveira, A.P.N.; Moreno, R. Synthesis of CaTiO₃ and CaTiO₃/TiO₂ nanoparticulate compounds through Ca²⁺/TiO₂ colloidal sols: Structural and photocatalytic characterization. *Ceram. Int.* **2018**, *44*, 301–309. [[CrossRef](#)]
94. Zhu, Y.; Zhu, D.; Yan, Q.; Gao, G.; Xu, J.; Liu, Y.; Alahakoon, S.B.; Rahman, M.M.; Ajayan, P.M.; Egap, E.; et al. Metal Oxide Catalysts for the Synthesis of Covalent Organic Frameworks and One-Step Preparation of Covalent Organic Framework-Based Composites. *Chem. Mater.* **2021**, *33*, 6158–6165. [[CrossRef](#)]
95. Zhang, M.; Lu, M.; Lang, Z.-L.; Liu, J.; Liu, M.; Chang, J.-N.; Li, L.-Y.; Shang, L.-J.; Wang, M.; Li, S.-L.; et al. Semiconductor/Covalent-Organic-Framework Z-Scheme Heterojunctions for Artificial Photosynthesis. *Angew. Chem. Int. Ed.* **2020**, *59*, 6500–6506. [[CrossRef](#)] [[PubMed](#)]